

THE ZIRCONIUM-RICH CORNER OF THE ZIRCONIUM-
TITANIUM-NIOBIUM CONSTITUTIONAL DIAGRAM

by

Bruce Cecil Whitmore

A thesis submitted in partial fulfilment of
the requirements for the degree of
MASTER OF APPLIED SCIENCE
in the Department
of
MINING AND METALLURGY

We accept this thesis as conforming to the
standard required from candidates for the
degree of Master of Applied Science.

Members of the Department
of Mining and Metallurgy

THE UNIVERSITY OF BRITISH COLUMBIA

January, 1958

ABSTRACT

An investigation of the zirconium-rich corner of the zirconium-titanium-niobium constitutional diagram is described. X-ray techniques and metallography were used. A high-temperature x-ray goniometer attachment was employed to construct ternary isopleths. Isothermal sections and lattice parameter measurements are also outlined. The occurrence of a transitional ω -phase identified tentatively as tetragonal, is noted. The ternary constitutional data presented represent essentially a survey of the zirconium-rich corner and more detailed results must await further work.

In presenting this thesis in partial fulfilment of the requirements for an advanced degree at the University of British Columbia, I agree that the Library shall make it freely available for reference and study. I further agree that permission for extensive copying of this thesis for scholarly purposes may be granted by the Head of my Department or by his representative. It is understood that copying or publication of this thesis for financial gain shall not be allowed without my written permission.

Department of Mining and Metallurgy,

The University of British Columbia,
Vancouver 8, Canada.

Date January 6th, 1958.

ACKNOWLEDGMENTS

The author is grateful for financial aid in the form of a research assistantship provided by the Defense Research Board of Canada under Research Grant DRB 7510-18.

The author gratefully acknowledges the assistance of Dr. V. Griffiths, the director of this research.

Special thanks are due to Mr. R.G. Butters for his design and construction of the high-temperature x-ray unit.

The technical advice and assistance of Mr. R. Richter and staff members are also acknowledged.

TABLE OF CONTENTS

	<u>Page</u>
I. INTRODUCTION	1
A. Purpose	1
B. The Three Binary Constitutional Diagrams	2
1. The Pure Metals	2
2. The Zirconium-Titanium Diagram	3
3. The Zirconium-Niobium Diagram	4
4. The Titanium-Niobium Diagram	8
II. EXPERIMENTAL	11
A. Alloy Preparation	11
B. Heat Treatments	14
C. Metallography	15
D. X-Ray Techniques	16
III. RESULTS	22
A. Metallographic Data	22
B. Lattice Parameters	26
C. Ternary Isopleths	27
D. Ternary Isothermals	33
IV. DISCUSSION OF RESULTS AND CONCLUSIONS	33
V. RECOMMENDATIONS FOR FURTHER WORK	45
VI. APPENDICES	
A. Related Binary Diagrams of Impurity Elements	46
B. Lattice Parameter Calculation by the Method of Cohen	52
C. d-Spacings of α -Containing Alloys and the ω -Phase	53
D. Temperature Determination of Phase Boundaries in One Low Niobium Alloy	56
VII. BIBLIOGRAPHY	57

LIST OF ILLUSTRATIONS

<u>Figure No.</u>	<u>Page</u>
1. The zirconium-titanium constitutional diagram	5
2. Lattice parameters of beta zirconium-titanium alloys	5
3. Lattice parameters of alpha zirconium-titanium alloys	6
4. The zirconium-niobium constitutional diagram	7
5. Lattice parameters of beta zirconium-niobium alloys	9
6. The titanium-niobium constitutional diagram	10
7. Lattice parameters of beta titanium-niobium alloys	10
8. Typical levitation melted-and-cast ingot	13
9. High-temperature x-ray unit furnace with a zirconium radiation shield and the external, water-cooled can	18
10. Specimen plate arrangement for the high-temperature x-ray unit	18
11. View of high-temperature x-ray unit showing the vacuum pumps, power supply, potentiometer and vacuum gauge	20
12. View of high-temperature x-ray unit showing the Geiger-counter scaler, rate meter and recorder	20
13. Lattice parameter versus temperature for hydrogen reduced copper powder as measured in the high-temperature x-ray unit	21
14. d-spacings of one plane versus temperature for pure silica as measured in the high-temperature x-ray unit	23
15. 85.4% Zr - 10.3% Ti - 4.3% Nb as-cast	24
16. Same equilibrated to 450°C	24
17. 76.9% Zr - 5.6% Ti - 17.6% Nb as-cast	24
18. Same equilibrated to 450°C	24
19. 85.4% Zr - 10.3% Ti - 4.3% Nb held at 600°C for 24 hours after 1 hour at 900°C.	25
20. Same held at 700°C for 24 hours after 1 hour at 900°C	25
21. 76.9% Zr - 5.6% Ti - 17.6% Nb held at 525°C for 70 hours after 1 hour at 900°C.	25
22. Same held at 600°C for 70 hours after 1 hour at 900°C	25

Illustrations (cont'd.)

<u>Figure No.</u>		<u>Page</u>
23.	64.8% Zr - 31.2% Ti - 4.0% Nb powder from high-temperature x-ray unit	26
24.	Variation of a and c for α phase in monotectoid alloys of low niobium content at 450°C	28
25.	Variation of a and c for α phase in monotectoid alloys of high niobium content at 450°C	28
26.	Variation of a_0 for β_{Nb} phase in monotectoid alloys of low niobium content at 450°C	29
27.	Variation of a_0 for β_{Nb} phase in monotectoid alloys of high niobium content at 450°C	29
28.	Ternary isopleth with niobium constant at 4.5 percent	30
29.	Ternary isopleth with niobium constant at 17.5 percent	30
30.	Sample scans showing the transformation of α to β	31
31.	Sample scans showing the monotectoid transformation	32
32.	Sample scans showing the growth of the transition ω -phase	32
33.	(a) Isothermal section at 800°C	34
	(b) Isothermal section at 750°C	35
	(c) Isothermal section at 700°C	36
	(d) Isothermal section at 650°C	37
	(e) Isothermal section at 600°C	38
	(f) Isothermal section at 550°C	39
	(g) Isothermal section at 500°C	40
	(h) Isothermal section at 450°C	41

LIST OF TABLES

<u>Table No.</u>		<u>Page</u>
1.	Some Approximate Physical Constants for Zirconium, Titanium and Niobium	2
2.	Typical Analysis of Crystal Bar Zirconium	11
3.	Typical Analysis of Crystal Bar Titanium	11
4.	Spectrographic Analysis of Niobium Rod	12
5.	Composition of Alloys Utilized	14
6.	Heat Treat Schedule for Two Alloys	15
7.	Etchants for Zirconium-Titanium-Niobium Alloys	16

THE ZIRCONIUM-RICH CORNER OF THE ZIRCONIUM-TITANIUM-NIOBIUM CONSTITUTIONAL DIAGRAM.

I. INTRODUCTION

A. Purpose

In the past ten years a large amount of research has been directed towards a study of the metallurgy of zirconium due to its applications in nuclear reactors. Some usages, however, have been limited by a low creep strength at high temperatures. Thus considerable effort has been made by many groups to determine experimentally the factors affecting the constitutional behaviour of zirconium. The development of versatile alloys follows more easily once such knowledge has been gained. This involves primarily the determination of constitutional diagrams as yet quantitatively unpredictable.

In an attempt to extend the knowledge it was decided to determine part of a ternary constitutional diagram of zirconium, utilizing titanium and niobium as the second and third components. Niobium was chosen as one component for it, too, has useful properties applicable to reactor core design. Titanium and niobium were also selected so that this research could be correlated with isothermal transformation kinetic studies being conducted on the zirconium-titanium-niobium system in the same Department.

The pure metals of the chosen system were also available and the desired alloys could easily be prepared by levitation melting techniques.

In addition to these factors, the three pertinent binary constitutional diagrams were reasonably well established and would provide a good guide. Also,

the zirconium-titanium system is theoretically important and the effect of a third element on that particular binary might then add more information of interest.

A literature search showed that no previous work had been reported on the system selected.

B. The Three Binary Constitutional Diagrams.

1. The Pure Metals.

The similarities between zirconium and titanium are extensive. Both metals have two allotropic modifications, low temperature alpha which is close-packed hexagonal and high temperature beta which is body-centered cubic. The transition temperatures are similar, 862°C in zirconium and 882°C in titanium. The melting points are also reasonably similar, 1845°C in zirconium and 1668°C in titanium. Niobium exists in the body-centered cubic modification at all temperatures below its melting point of 2415°C. Table 1 compares approximate values for some physical constants of zirconium, titanium and niobium.

Table 1

Some Approximate Physical Constants for Zirconium, Titanium and Niobium¹

Property	Zirconium	Titanium	Niobium
α phase (cph)			
a ₀ (Å)	3.230	2.950	-
c ₀ (Å)	5.133	4.683	-
c ₀ /a ₀	1.589	1.593	-
β phase (bcc)			
a ₀ (Å at 20°C)	3.59 (extrapolated)	3.285 (extrapolated)	3.301
Atomic No.	40	22	41
Atomic Wt.	91.22	47.90	92.91
Dist. of closest Approach (Å)	3.17 (α)	2.89 (α)	2.859
Density (gm/cc.)	6.50	4.54	8.57

Zirconium is a member of the second transition series of elements and has two 4 d electrons in the incomplete electronic shell. Titanium, its sister element of the first transition series, has two 3 d electrons in its outer shell. Niobium, one atomic number above zirconium, has ~~one~~^{four} 4 d electrons.

The theoretical and experimental alloying behaviour of zirconium has been extensively reviewed by Pfeil^{2, 3}. One of the principal features of his theoretical review was his attempt to extrapolate results gained from titanium constitutional diagrams to zirconium systems. This was possible because of the similarities pointed out and many reasonable predictions were made.

Of particular interest in constitutional diagram studies is the effect of impurity elements on the diagrams. The major contaminants encountered in this work were oxygen, nitrogen and hafnium. Oxygen and nitrogen pick-up can be avoided only when the best high-vacuum or inert atmosphere techniques are used. The hafnium content of the alloys appeared to be of little consequence as it is completely soluble in both titanium and zirconium.

It is well known that both zirconium and titanium take oxygen and nitrogen into solution extensively and that no high temperature vacuum treatment can outgas the two metals. The effect on the transformation temperature of both metals is serious, as small amounts of oxygen and nitrogen will stabilize the alpha phase to the melting point. Lesser amounts alter the transformation temperature radically. The related binary diagrams of these impurity elements are presented in Appendix A.

2. The Zirconium-Titanium Diagram.

The zirconium-titanium constitutional diagram exhibits a complete series of isomorphous solid solutions in both the alpha and beta fields. The

diagram presented in Figure 1 represents the work of Fast⁴ with slight modifications by Hayes et al.⁵ A minimum in the alpha-beta transformation temperature occurs at 50 atomic percent. On the assumption that the valencies of zirconium and titanium are the same, this result cannot be explained as a Brillouin zone effect. Nor can any obvious d-shell interaction effect be suggested. Lattice parameter plots, as in Figures 2 and 3, are linear for both alpha and beta zirconium-titanium alloys and this suggests that ordering effects are not operative. If the depression is real, a true explanation for it must be found as one is necessary for a proper theoretical understanding of the zirconium alloy systems.

The reaction rates for this system are extremely fast. Duwez⁶ found no depression of the transformation temperatures suggested by the equilibrium diagram of Fast with cooling rates up to 8000°C/sec. At this rate, beta phase could be only partially retained in alloys ranging from 30 to 70 atomic percent titanium.

3. The Zirconium-Niobium Diagram.

The diagram determined by Rogers and Atkins⁷ is given in Figure 4. The diagram exhibits a complete series of isomorphous solid solutions in the beta field from the melting points to a temperature of approximately 980°C. At this temperature, the critical point for a region of beta solid solution immiscibility occurs; the composition parameter being approximately 63 percent niobium. At lower temperatures to 615°C, the alloys between 17.5 to 87.0 percent niobium decompose to beta zirconium and beta niobium. Alloys from 6.7 to 17.5 percent niobium decompose to alpha plus beta zirconium between 862°C and 615°C. At 615°C, alloys from 6.7 to 87.0 percent niobium decompose monotectoidally to a monotectoid of alpha zirconium and beta niobium. A small region of alpha solid solubility exists up to 6.7 percent niobium at the

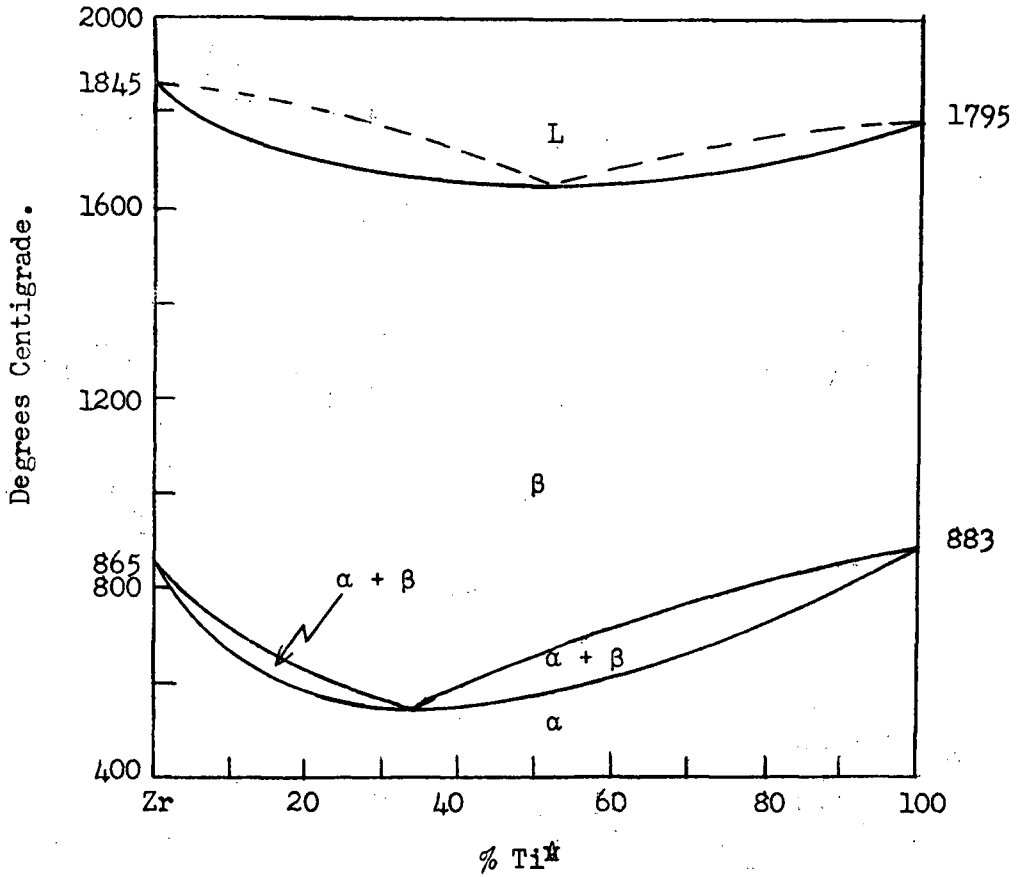


Figure 1. The zirconium-titanium constitutional diagram (after Fast⁴ and Hayes et al⁵)

* Weight percentages are used throughout unless otherwise stated.

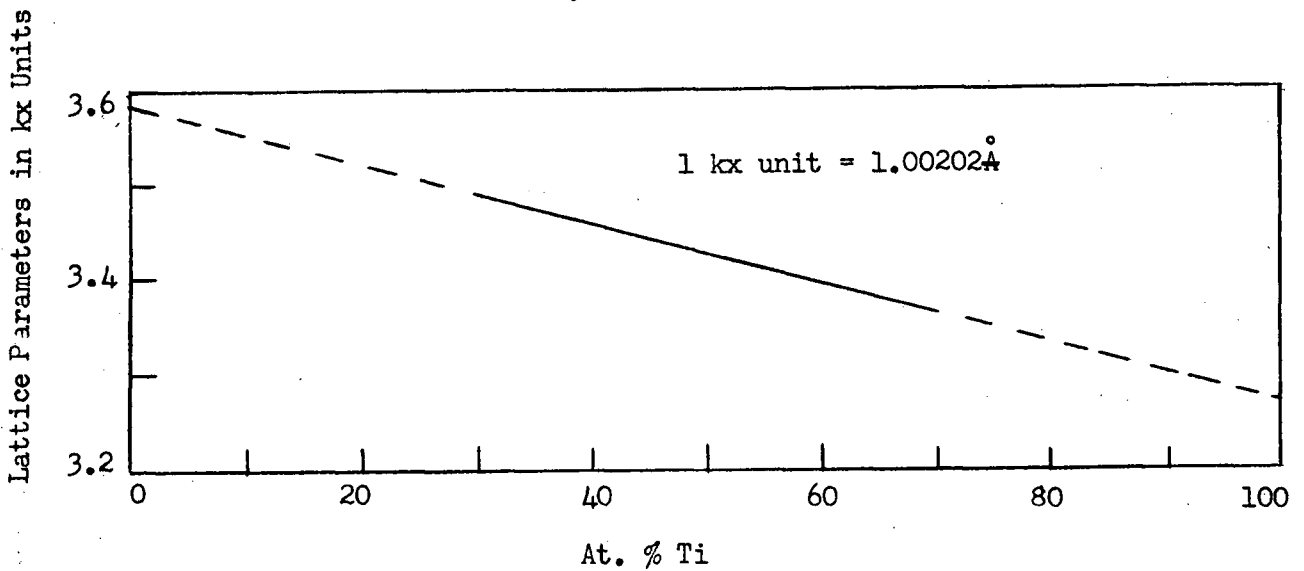


Figure 2. Lattice parameters of beta zirconium-titanium alloys (after Duwez⁶).

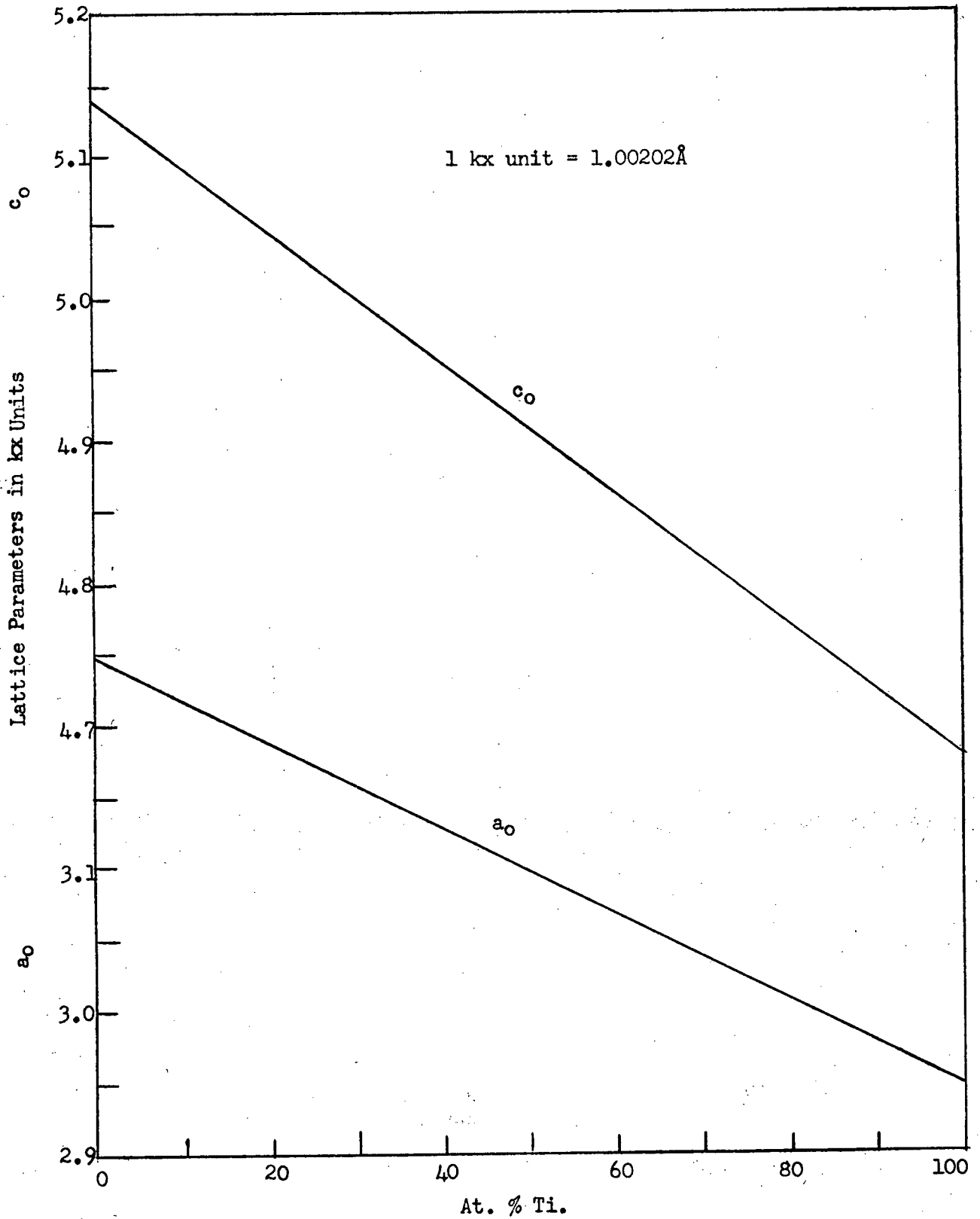


Figure 3. Lattice parameters of alpha zirconium-titanium alloys (after Fast⁴ and Duwez⁶).

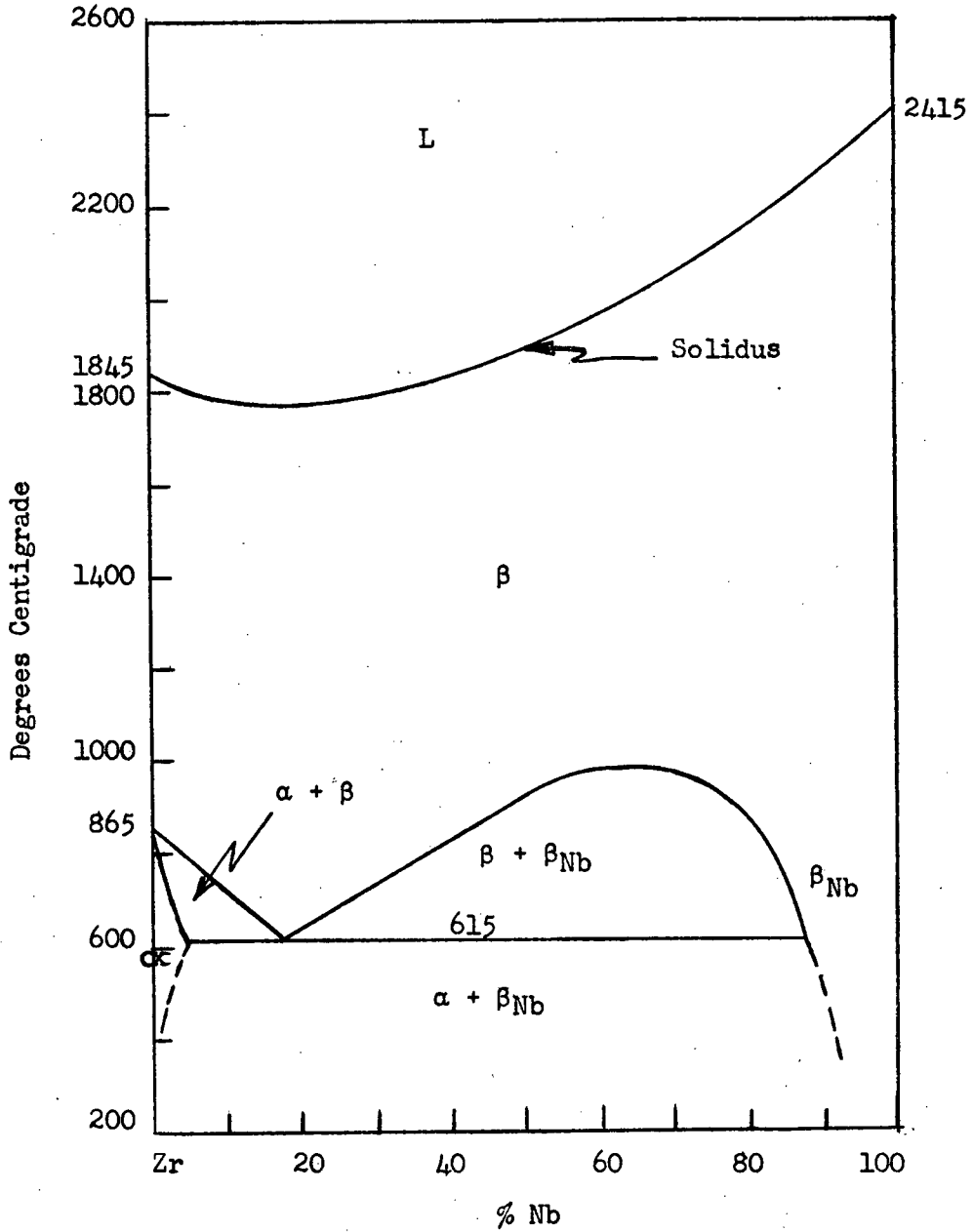


Figure 4. The zirconium-niobium constitutional diagram (after Rogers and Atkins⁷).

monotectoid temperature.

A short time after the diagram of Rogers and Atkins was incorporated into this work, a slightly different diagram was published by Bychkov et al.⁸ The principal difference contained in their diagram was that the monotectoid occurred at 550°C. This difference was not supported by this research and so the diagram of Rogers and Atkins was still considered to be the best available.

Rogers and Atkins also reported the lattice parameters for the region of complete beta solid solubility and this information is shown in Figure 5.

The reaction rates in this system are of reasonable speed. Alloys of less than 15 percent niobium undergo some transformation on quenching from 1100°C and, for those above 15 percent, the beta phase can be completely retained to room temperature. The work of Finlayson⁹ outlined beta to monotectoid decomposition rates that were reasonably rapid.

4. The Titanium-Niobium Diagram.

The titanium-niobium diagram determined by Hansen et al¹⁰ is shown in Figure 6. The diagram exhibits a complete series of isomorphous solid solutions across the beta field whereas niobium is only slightly soluble in the alpha titanium modification. The lattice parameters for beta titanium-niobium alloys as reported by Hansen et al are shown in Figure 7.

The investigators found that with alloys containing more than 25 percent niobium residual coring could not be removed no matter how severely the alloys were cold worked and no matter how long they were homogenized. This was principally due to the extremely sluggish reaction rates encountered and for this reason, the diagram was not accurately determined below 650°C. Such slow reactions do not affect this work materially as the titanium-niobium system is

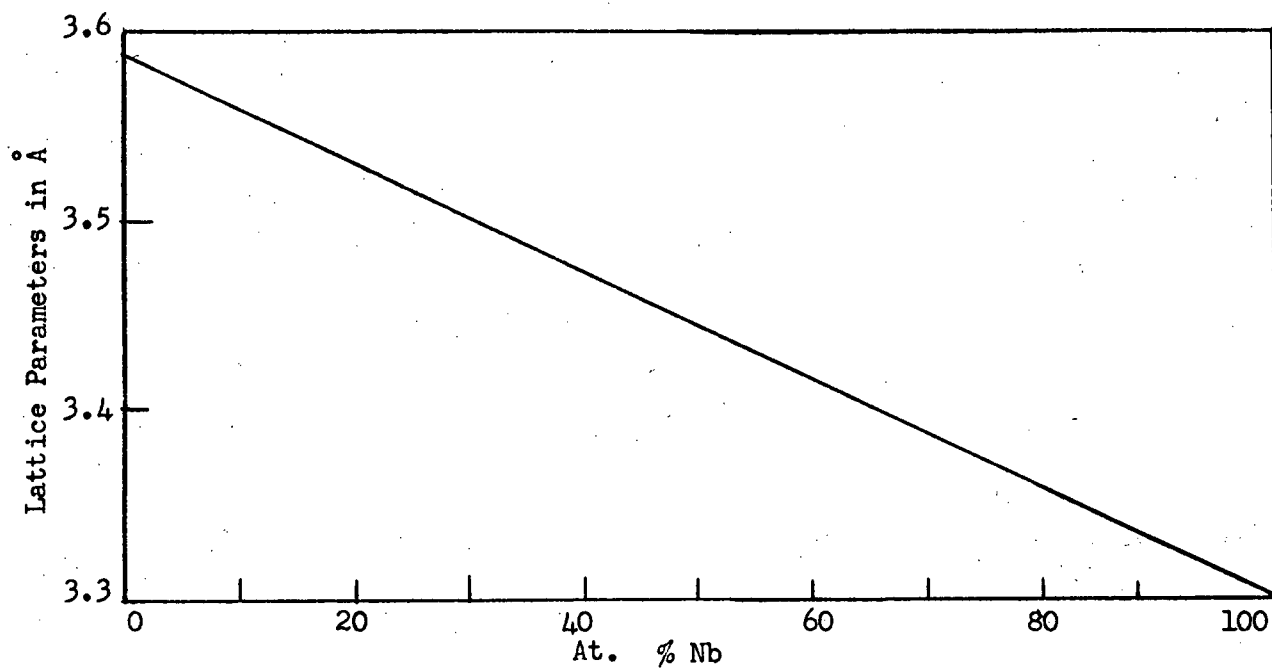


Figure 5. The lattice parameters of beta zirconium-niobium alloys (after Rogers and Atkins⁷).

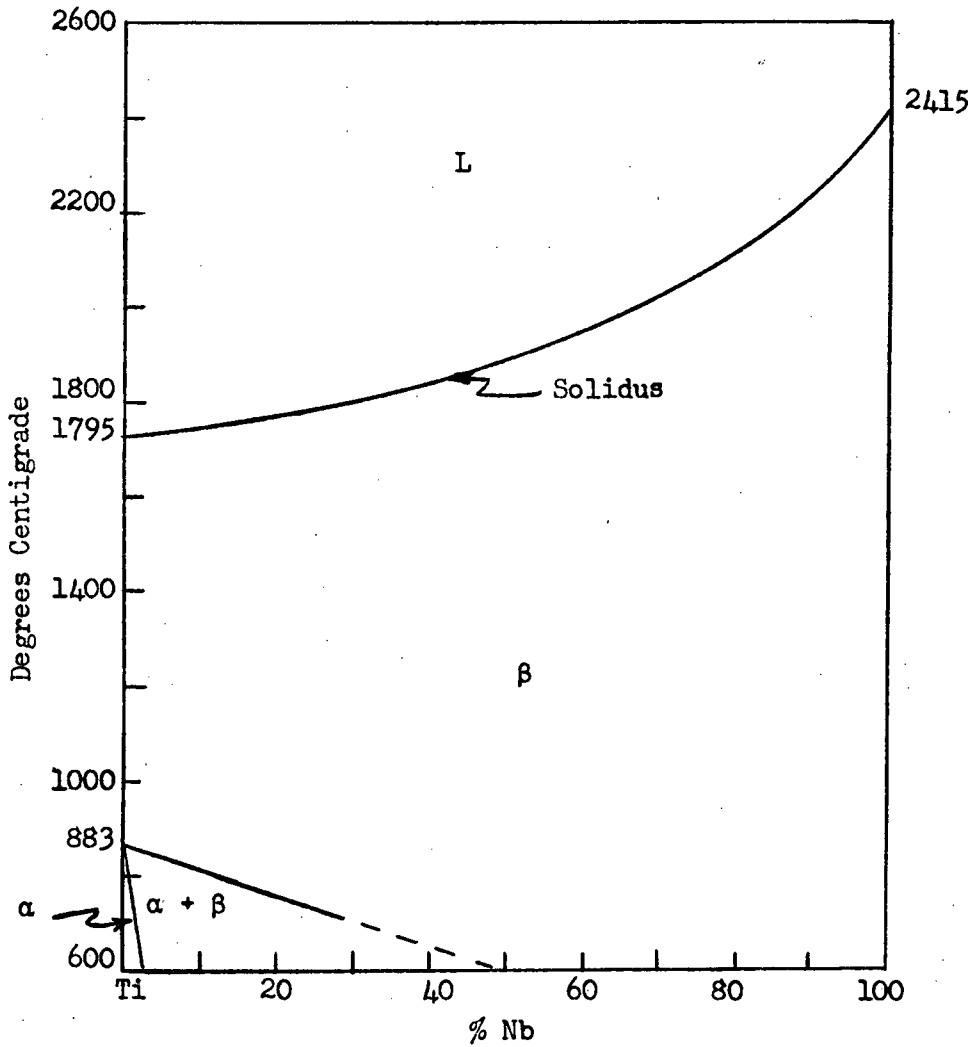


Figure 6. The titanium-niobium constitutional diagram (after Hansen et al.¹⁰).

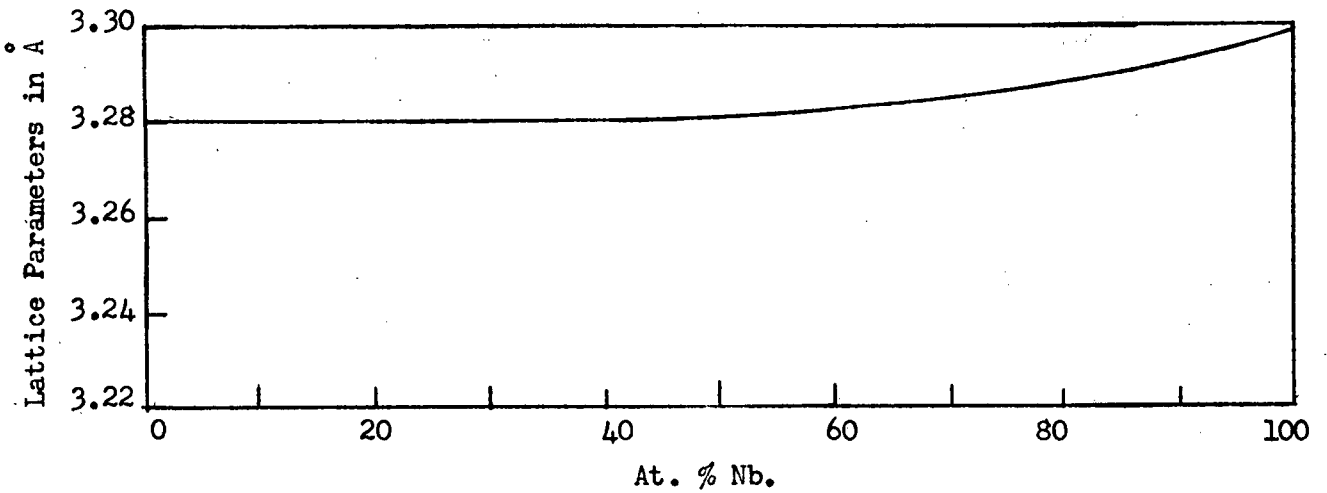


Figure 7. Lattice parameters for beta titanium-niobium alloys (after Hansen et al.).

the minor side of the ternary diagram under consideration.

II EXPERIMENTAL

A. Alloy Preparation.

The zirconium metal used in the alloys was iodide crystal bar supplied by the Foote Mineral Company. Table 2 gives the reported analysis of the bar from which all alloys were made.

Table 2.

Analysis of Crystal Bar Zirconium.

Element	Weight Percent
Hf	2.17
Si	0.005
Al	0.002
Mn	0.001
Mg	0.002
Fe	0.002
Cr	0.001
Ti	0.006
Ni	trace
Ca	0.003
Cu	0.0005
O ₂	0.01

The titanium metal used was in the form of iodide crystal bar supplied by A.D. McKay Company. No specific analysis was available and so a typical analysis is quoted in Table 3.

Table 3.

Typical Analysis of Crystal Bar Titanium¹¹

Element	Weight Percent
O ₂	0.01
N ₂	0.005
C	0.03
Fe	0.04
Ca	trace
Al	0.05
Si	0.03
Pb	trace
Ni	trace
Mo	trace

The niobium metal used was in the form of 4.7 mm. diameter rods supplied by Johnson, Matthey and Company. An exact spectrographic analysis of the rods supplied is given in Table 4.

Table 4.

Spectrographic Analysis of Niobium Rod.

Element	Weight Percent
Ta	0.5
Ni	0.0007
Fe	0.004
Ti	0.012

Melt stock was prepared by sawing slices from the respective metal bars. A small hole was drilled in each slice and then all were cleaned in acetone. Each slice composing a ternary alloy was then carefully weighed and finally tied into a bundle utilizing the small holes and 0.005 inch zirconium wire. The bundle was then cleaned a second time in acetone.

All alloys were melted and cast by the levitation melting technique previously described by Polonis et al.¹² Some changes were required for the satisfactory melting of zirconium alloys, the most significant being a slightly different coil than that used by Polonis for the melting of titanium alloys. The coil design adopted was that used by Finlayson⁹ and after proper alignment any alloy desired up to 20 percent niobium could be melted with ease. The power supply used was a 23.5 Kva Lepel valve oscillator.

A second departure from the original practice established by Polonis was the use of purified helium instead of argon as the inert atmosphere and at a pressure of 15 psig instead of 5 psig to reduce power arcing from the coil to the specimen. The helium was purified by passing it over activated charcoal at a pressure of 40 psig and at liquid nitrogen temperature.

The alloy bundle was suspended in the center of the levitation coil by means of the 0.005 inch zirconium wire which was attached to a glass hook in the top plate of the chamber. After evacuating the chamber and backfilling with helium three times to the pressure mentioned, the power was quickly turned up to 100 percent output. When the specimen had melted and was judged to be sufficiently hot and thoroughly mixed, the power was slowly cut back, which effectively poured the molten alloy into the copper mold. A typical ingot is shown in Figure 8.

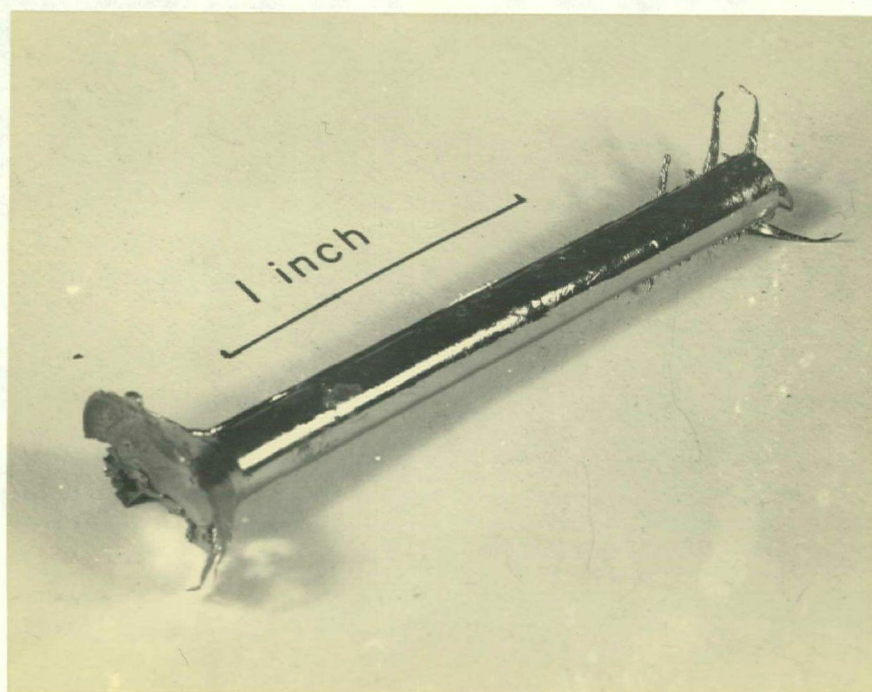


Figure 8. Typical levitation melted-and-cast ingot.

One check with an optical pyrometer gave a temperature of 2500°C just prior to casting. At this temperature a black vapour was given off and was presumed to come from the molten zirconium and titanium as these two metals have fairly high vapour pressures at such temperatures.

All specimens so melted were bright and clean on removal from the mold. Weighing in and out gave a difference of ± 2 mg for a weigh-in of approximately 6.5 gms for each alloy. In the absence of chemical analyses,

the weights of each element in an alloy must therefore represent the composition of each alloy. Table 5 lists the ten alloys on which this research was based. A further seven alloys were rejected due to gas contamination either from melting or heat treatment.

Table 5.

Composition of Alloys Utilized.

Alloy	% Zr	% Ti	% Nb
T-8	90.0	5.3	4.7
T-9	85.4	10.3	4.3
T-10	79.0	16.4	4.6
T-11	74.0	21.5	4.5
T-12	64.8	31.2	4.0
T-13	76.9	5.6	17.6
T-14	73.5	9.4	17.2
T-15	68.5	14.4	17.0
T-16	63.1	19.8	17.1
T-17	55.4	27.3	17.4

Slices were removed from the as-cast ingots for metallographic examination using a two-zero jeweler's hacksaw. The saw filings were collected for x-ray powder diffraction experiments. Iron from the saw blades was removed from all filings with a small magnet.

B. Heat Treatments.

The as-cast ingots were subjected to a constant, slight amount of compressive cold work to break up the as-cast structure. All ingots were wrapped in molybdenum sheet and placed in vitreosil bulbs containing zirconium getter chips. The bulbs were then evacuated and sealed off. Each bulb was heated to 1000°C for 48 hours to promote homogenization and was then cooled at a rate of 100°C per day until a temperature of 450°C was reached. At this temperature, the capsules were held for a further 48 hours and then water quenched to preserve the structure at 450°C. The structures attained were

considered to be the equilibrium ones for 450°C.

Slices were taken from each ingot for metallographic examination and the saw filings were collected as before.

Slices from one low- and one high-niobium ingot were then given the heat treatments outlined in Table 6.

Table 6.
Heat Treat Schedule for Two Alloys.

85.4% Zr-10.3% Ti-4.3% Nb	76.9% Zr-5.6% Ti-17.6% Nb
3 pieces 1 hr. at 900°C	3 pieces 1 hr. at 900°C
then 1 piece 24 hrs. at 600°C.	then 1 piece 70 hrs. at 525°C
and 1 piece 24 hrs. at 700°C	and 1 piece 70 hrs. at 600°C.
and 1 piece 24 hrs. at 800°C.	and 1 piece 70 hrs. at 675°C.

The tube furnaces used for the above list treatments were all checked with a secondary standard platinum/platinum-10 percent rhodium thermocouple and all were found to control within ±5°C of the control point.

Upon examining these specimens metallographically, it was possible to outline the phase boundaries roughly.

The saw filings obtained from the homogenized and equilibrated ingots were wrapped in molybdenum sheet and placed in Pyrex bulbs along with zirconium getter chips. The bulbs were then evacuated and sealed off. These bulbs were next held at 450°C for 70 hours to strain relieve the saw filings without destroying the equilibrium structure.

C. Metallography.

All specimens examined were polished on number two through to number

four-zero emery papers. The specimens were preliminary lapped on waxed billiard cloth using levigated 600x alundum.. Final lapping was done on micro-cloth using Linde B levigated alumina.

Etching the specimens was somewhat difficult and a considerable amount of time and effort was required before suitable etchants were devised (by trial and error) to portray the structures adequately. In particular, alloys exhibiting a monotectoid structure were very awkward to handle. Table 7 lists the various etchants developed. Because of this difficulty, metallography has

Table 7

Etchants for Zirconium-Titanium-Niobium Alloys.

As-cast Structures	Heat Treated Structures
<u>Chemical Polish No. 1</u> 20 mls HNO ₃ 30 mls lactic acid 10 drops HF <u>Etch No. 1</u> 20 mls HNO ₃ 20 mls HF 60 mls glycerine	<u>Etch No. 2</u> 20 mls HNO ₃ 30 mls lactic acid 30 mls glycerine 6 drops HF

been used only as a qualitative tool and x-ray techniques were depended upon to give quantitative results.

D. X-Ray Technique.

Lattice parameters and d-spacings were determined for all alloys equilibrated to 450°C by taking powder pictures of strain relieved saw filings obtained from heat treated ingots. A 114.6 mm. diameter Debye-Scherrer powder camera was used with the film mounted in the Straumanis position. A nickel filter was also incorporated inside the camera between the specimen and the

film to reduce the strong fluorescent radiation. Copper K_{α} radiation was utilized with the tube operating at 40 Kv and 15 ma. Exposures of three hours were required to obtain satisfactory results.

Lattice parameters for close-packed hexagonal crystal structures were calculated by the method of Cohen as indicated in Appendix B. Parameters for body-centered cubic phases were determined by extrapolating a plot of a_0 versus Taylor-Sinclair function to $\theta = 90^\circ$.

The quantitative results presented in this thesis are based on high-temperature x-ray goniometer plots. Butters and Parr¹³ had built a high-temperature attachment to fit a Phillips high-angle x-ray diffraction goniometer that relied upon an inert atmosphere to prevent specimen contamination. Their platinum furnace was wound on a vitreosil tube and this was believed to be the source of gas contamination that they encountered. To handle reactive zirconium alloy powders, it was decided to redesign the high-temperature unit and utilize a high-vacuum system to prevent gas contamination. As much refractory material as possible was eliminated from the vacuum system.

The furnace was wound from 0.010 inch zirconium wire with the wire strung longitudinally from molybdenum hooks which in turn were insulated from the stainless steel end rings by small ceramic beads. Figure 9 shows the furnace with a zirconium radiation shield in position and the external, water-cooled can. The zirconium winding and radiation shield provided a self-gettering action that improved the vacuum appreciably.

The powder specimen was placed on a molybdenum specimen plate which in turn was sprung onto a molybdenum rod harp. Provisions were made to align the



Figure 9. High-temperature x-ray unit furnace with a zirconium radiation shield and the external, water-cooled can.

harp accurately with the goniometer system. The platinum/platinum - 10 percent rhodium thermocouple dipped into the powder on the specimen plate. Figure 10

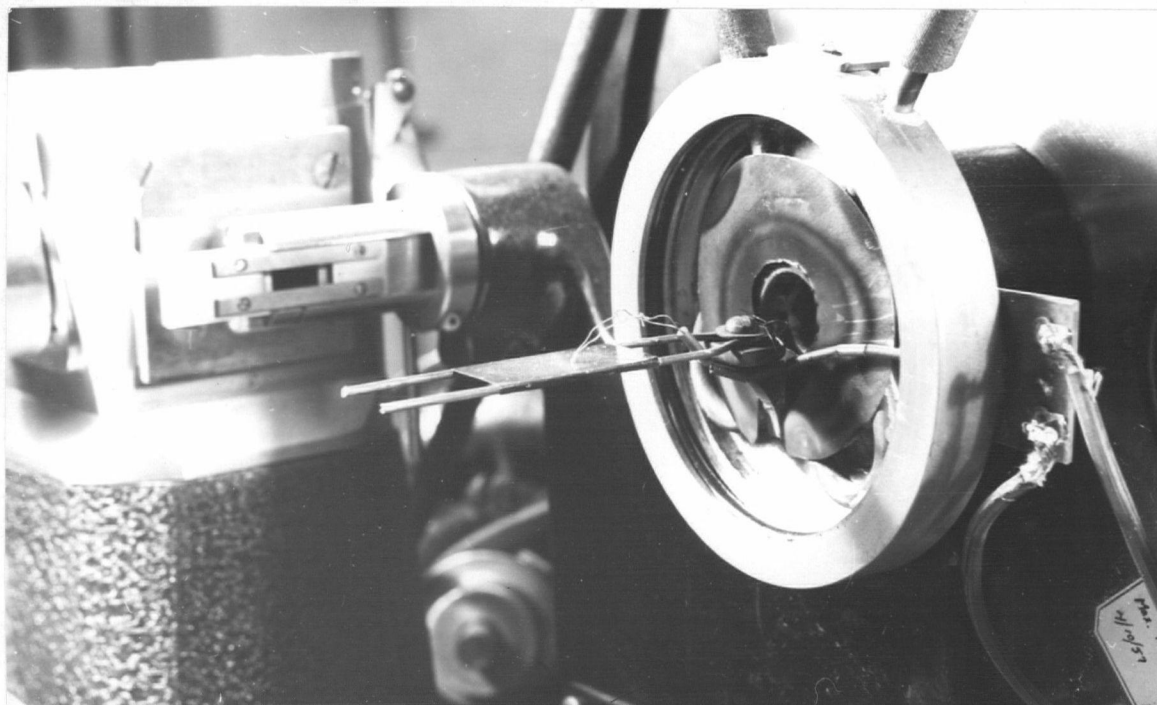


Figure 10. Specimen plate arrangement for the high-temperature x-ray unit.

shows the specimen plate arrangement.

A further innovation was the use of 0.001 inch nickel foil window for the entry and exit of x-rays to the evacuated can. The earlier aluminum foil windows developed leaks after short use and were therefore not dependable. The nickel foil served both as a CuK_β radiation filter and a vacuum tight window. It was soft-soldered into position and can be seen in several of the photographs. Figures 11 and 12 show the experimental apparatus in operation.

The vacuum pumping system consisted of a liquid nitrogen trap, a VMF-10, air-cooled oil diffusion pump and a Welch Duo-Seal 1400B backing pump. A pressure of 10^{-6} mm. of mercury was easily maintained at high temperatures. The vacuum pressure was measured with an NRC ion gauge.

The temperature was controlled directly by means of the Variac and limits of $\pm 5^\circ\text{C}$ were easily held. The thermocouple was calibrated by two independent methods. The first calibration was accomplished by measuring the lattice parameter of Sherritt-Gordon hydrogen reduced copper powder with increasing temperature. The curve obtained in Figure 13 was then compared with the expression for the coefficient of thermal expansion for pure copper. The equation is:

$$L_t = L_0 \left[1 + (16.733t) \times 10^{-6} \right]$$

This calibration showed the thermocouple to be without error. However, the expression above demands an accuracy which was not attained in the lattice parameter measurements utilized and an error of 10°C would likely not be noticeable.

The second calibration eliminated this uncertainty as a material exhibiting a transformation was utilized. Pure crystalline quartz was suitable

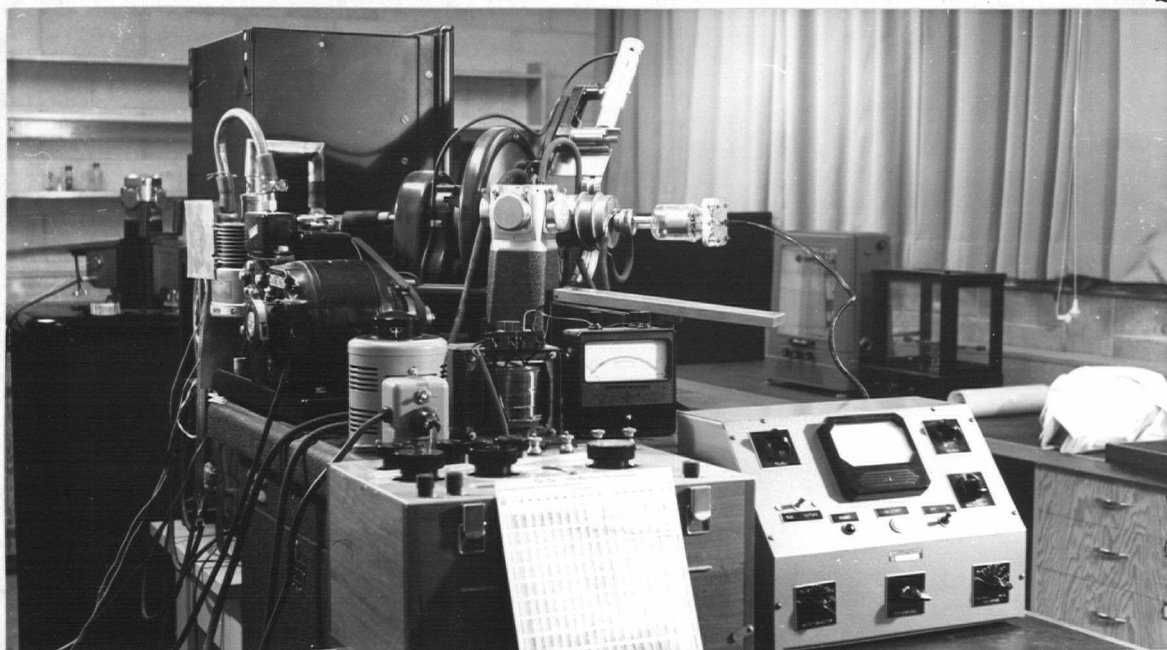


Figure 11. View of high-temperature x-ray unit showing the vacuum pumps, power supply, potentiometer and vacuum gauge.



Figure 12. View of high-temperature x-ray unit showing the Geiger-counter scaler, rate meter and recorder.

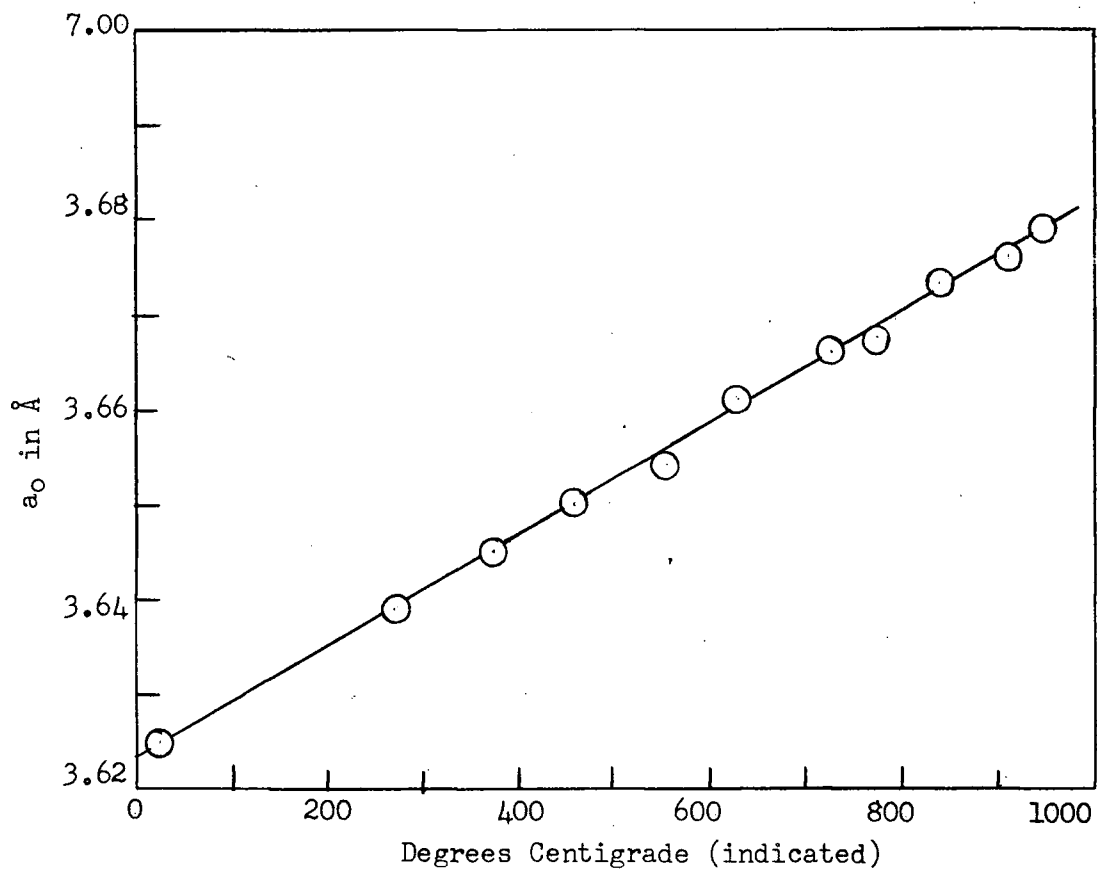


Figure 13. Lattice parameter versus temperature for hydrogen reduced copper powder as measured in the high-temperature x-ray unit.

as it has a sharp lattice expansion at 573°C. Accordingly, the d-spacings for one plane of a silica specimen versus temperature were obtained and the resulting curve is shown in Figure 14. A hysteresis of 10°C was encountered and as the cooling and heating rates were roughly equal, the true transformation temperature was taken to be the average, which gave a true temperature of 585°C. The thermocouple was thus in error by +12°C and this error was subsequently subtracted from the indicated temperatures utilized for the determination of the ternary isopleths.

III RESULTS

A. Metallographic Data

Figures 15, 16, 17 and 18 show photomicrographs that were completely typical of all specimens. Two groups were apparent; low niobium alloys had equivalent structures and high niobium alloys had equivalent structures for any given heat treatments.

The needle-like markings in the as-cast specimens remain unidentified,⁹ but are suspected to be hydrides. No extra lines were visible in x-ray powder pictures of the as-cast powders. Further information on their nature must await micro-beam x-ray experiments being conducted at Chalk River.

Figures 19, 20, 21 and 22 are photomicrographs of the slices used to outline the ternary phase boundaries roughly. Figure 20 demonstrates that the $\beta/\alpha + \beta$ boundary must lie below 700°C. Figure 22 demonstrates that the $\beta/\alpha + \beta_{\text{Nb}}$ boundary must lie below 600°C. This was the extent of the metallographic work and it will be shown that the x-ray results compare favourably with these data.

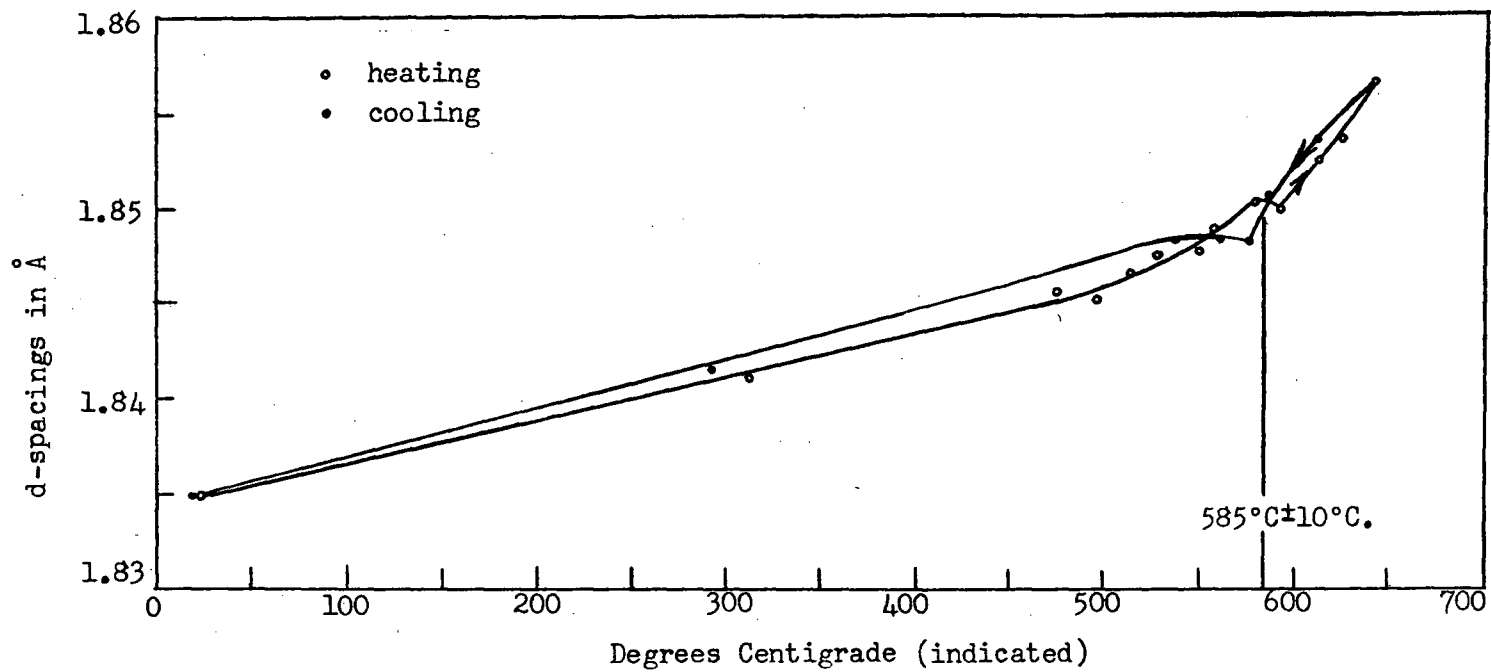


Figure 14. d-spacings of one plane versus temperature for pure silica as measured in the high temperature x-ray unit.



Figure 15 85.4% Zr-10.3% Ti-4.3% Nb
as-cast. Transformed β ,
i.e., α' . Chemical polish
No. 1. Etch No.1 x 800



Figure 16 Same equilibrated to
450°C. α .
Etch No. 2 x 800.

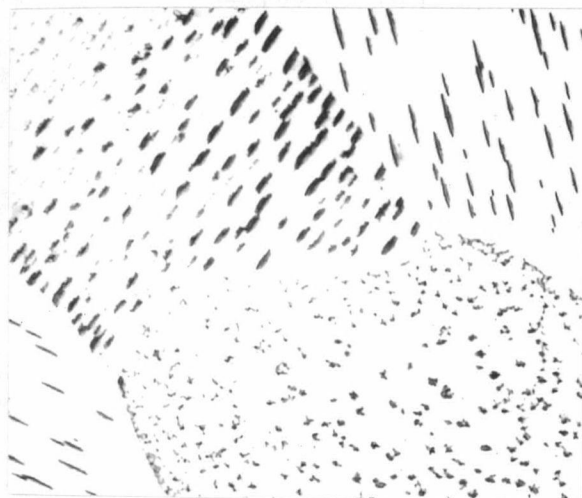


Figure 17 76.9% Zr-5.6% Ti-17.6% Nb
as-cast. Retained β +
unidentified needles.
Chemical polish No. 1.
Etch No. 1 x 800.

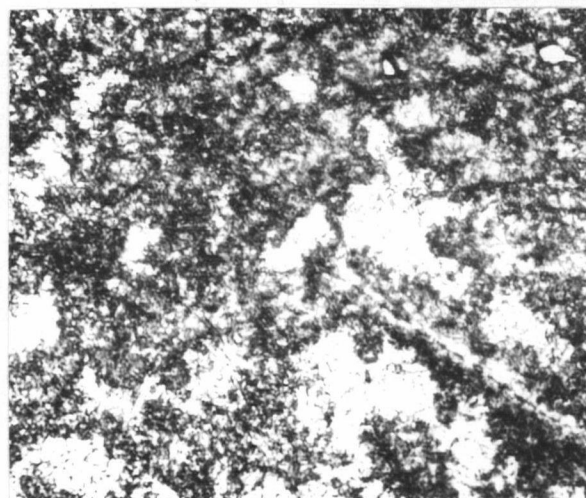


Figure 18 Same equilibrated to
450°C. Monotectoid
 $\alpha + \beta$ Nb.
Etch No. 2 x 800.

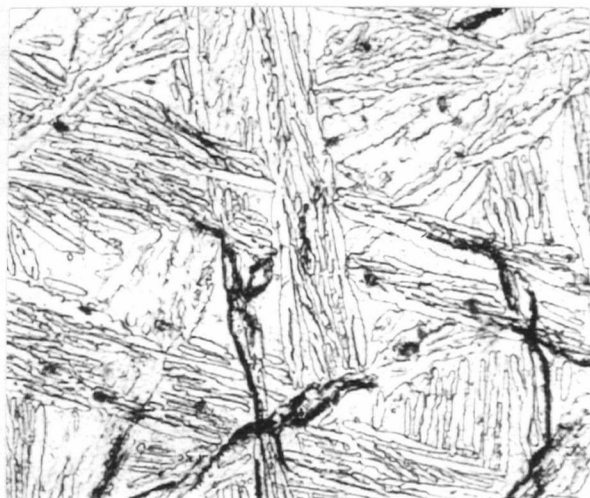


Figure 19 85.4% Zr-10.3% Ti-4.3% Nb
held at 600°C for 24 hours
after 1 hour at 900°C. α .
Etch No. 2 x 800



Figure 20 Same held at 700°C for
24 hrs. after 1 hr. at
900°C. Transformed β .
Etch No. 2 x 800.

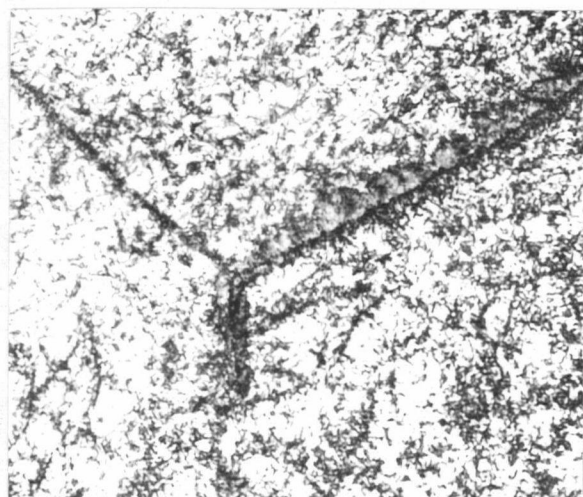


Figure 21 76.9% Zr-5.6% Ti-17.6% Nb
held at 525°C for 70 hrs.
after 1 hr. at 900°C.
 $\alpha + \beta_{Nb}$.
Etch No. 2 x 800

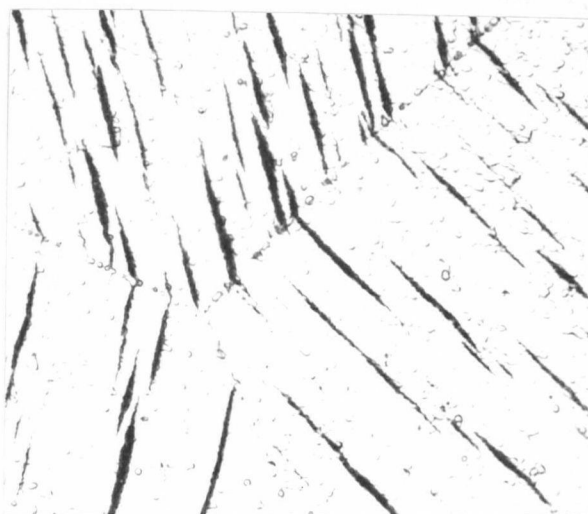


Figure 22 Same held at 600°C for
70 hrs. after 1 hr. at
900°C. Retained β
+ needles.
Etch No. 2 x 800.

Figure 23 is a photomicrograph of powder taken from the high-temperature x-ray unit. The powder was heated to 900°C and then was being cooled at the rate of 100°C per hour in an attempt to observe the $\beta/\alpha + \beta$

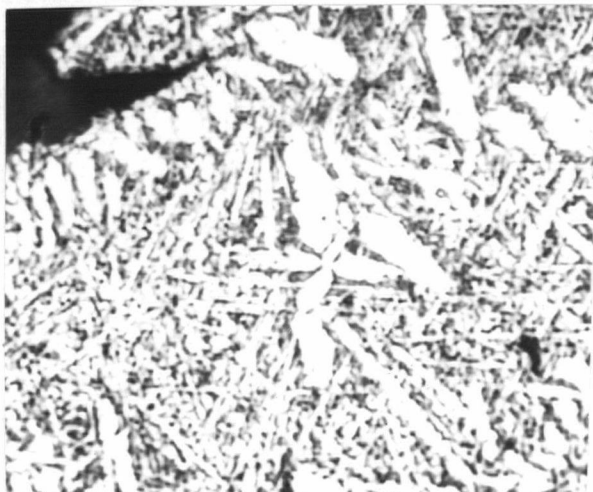


Figure 23. 64.8% Zr-31.2% Ti-4.0% Nb powder from the high-temperature x-ray unit. $\alpha +$ retained $\beta + x$. Etch No.2 x2500

phase change. Unexpectedly an unidentified phase began to precipitate, and the experiment was terminated by a rapid cooling to room temperature. An x-ray powder picture showed three phases to be present; α , retained β , and the unidentified phase. The photomicrograph was included to point out the difficulties encountered when visual identification was attempted.

B. Lattice Parameters

The d-spacings for all α -containing alloys equilibrated to 450°C are given in Appendix C and are compared to the National Bureau of Standards d-spacings for pure zirconium. Included also in Appendix C is a table of d-spacings for the unidentified phase mentioned above and its tentative identification. Nearly all powder films contained some faint extra lines that could not be indexed.

Figures 24 and 25 show the variation of c and a for increasing atomic percent titanium. The 64.8% Zr-31.2% Ti-4.0% Nb alloy parameters were not plotted in Figure 24 as its structure was nearly 100 percent β at the temperature considered with some weak α phase lines. This will also be shown in the ternary isopleth determined for the 4.5 percent niobium alloys. The 55.4% Zr-27.3% Ti-17.4% Nb alloy parameters were not plotted in Figure 25 for the same reason.

Figures 26 and 27 show the lattice parameters for the β_{Nb} phase of the monotectoid. If Vegard's law is obeyed for the ternary system, then it can be shown that the β_{Nb} parameter for the 64.8% Zr-31.2% Ti-4.0% Nb alloy is equal to the parameter predicted by Vegard's law for the region of β solid solubility. The same is nearly true for the 55.4% Zr-27.3% Ti-17.4% Nb alloy.

C. Ternary Isopleths

The term 'isopleth' denotes a ternary vertical section that either originates in one corner of the ternary triangle and thus has a constant ratio of second to third components or is parallel to one side of the ternary triangle and thus has one component constant.¹⁴

The two ternary isopleths presented in Figures 28 and 29 were constructed entirely from data obtained from the high-temperature x-ray unit. The isopleth in Figure 28 has a constant niobium content of approximately 4.5 percent. The one in Figure 29 has a constant niobium content of approximately 17.5 percent. Both isopleths were constructed by heating and cooling alloy powders in the high-temperature x-ray unit and observing the growth and decomposition of the various phases present. The low niobium isopleth consists of β decomposing to $\alpha + \beta$ which decomposed in turn to $\alpha + \beta_{\text{Nb}}$. The exact temperatures of the phase boundaries presented were obtained by plotting peak intensities versus temperature and extrapolating to zero peak intensity.

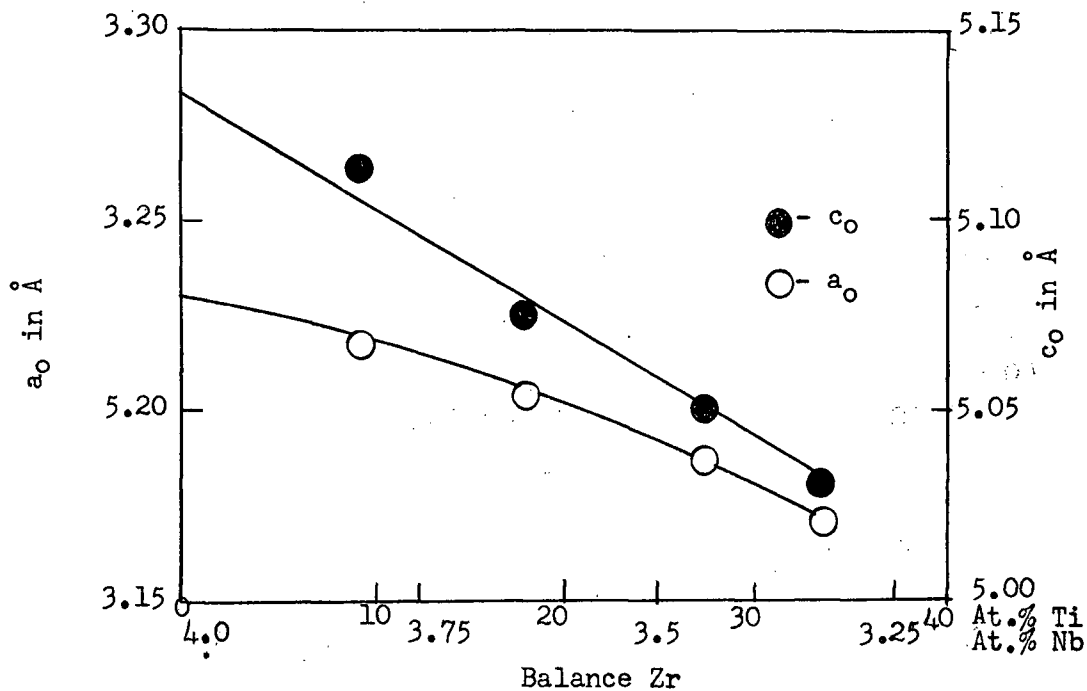


Figure 24. Variation of c and a for α phase in monotectoid alloys of low niobium content at 450°C.

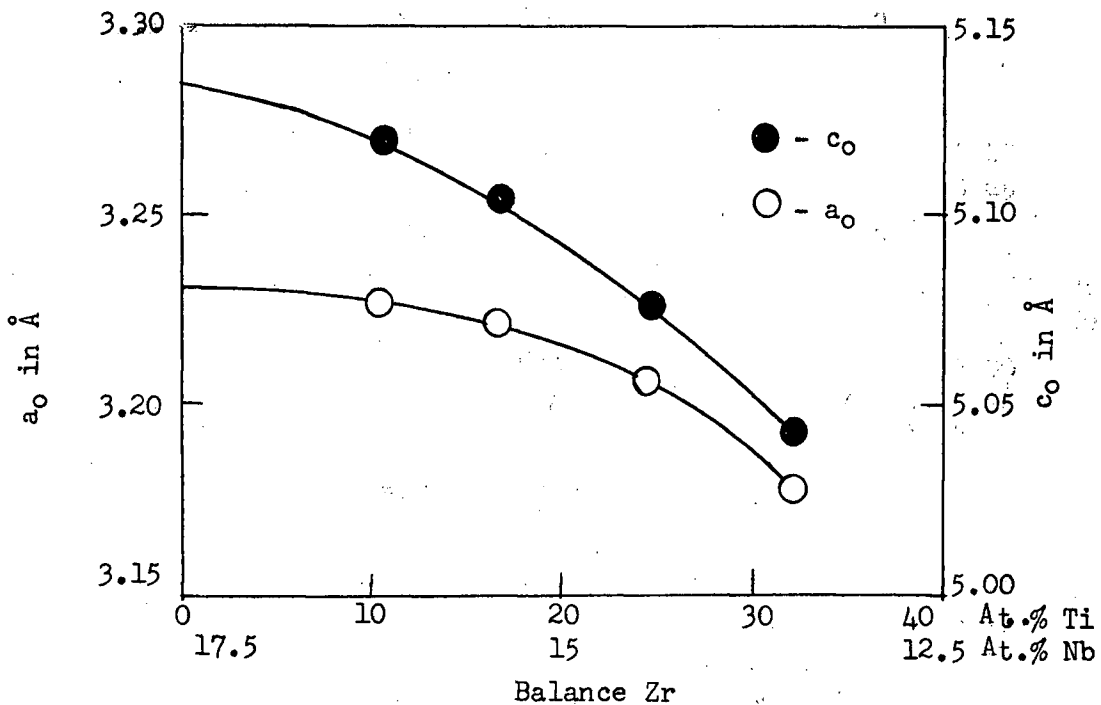


Figure 25. Variation of c and a for α phase in monotectoid alloys of high niobium content at 450°C.

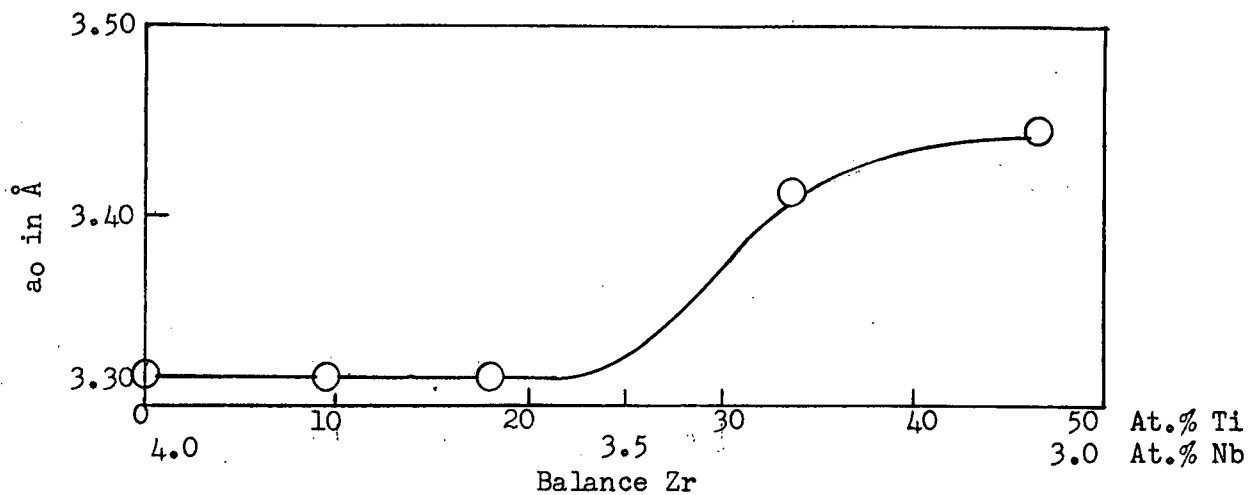


Figure 26. Variation of a_0 for β_{Nb} phase in monotectoid alloys of low niobium content at 450°C.

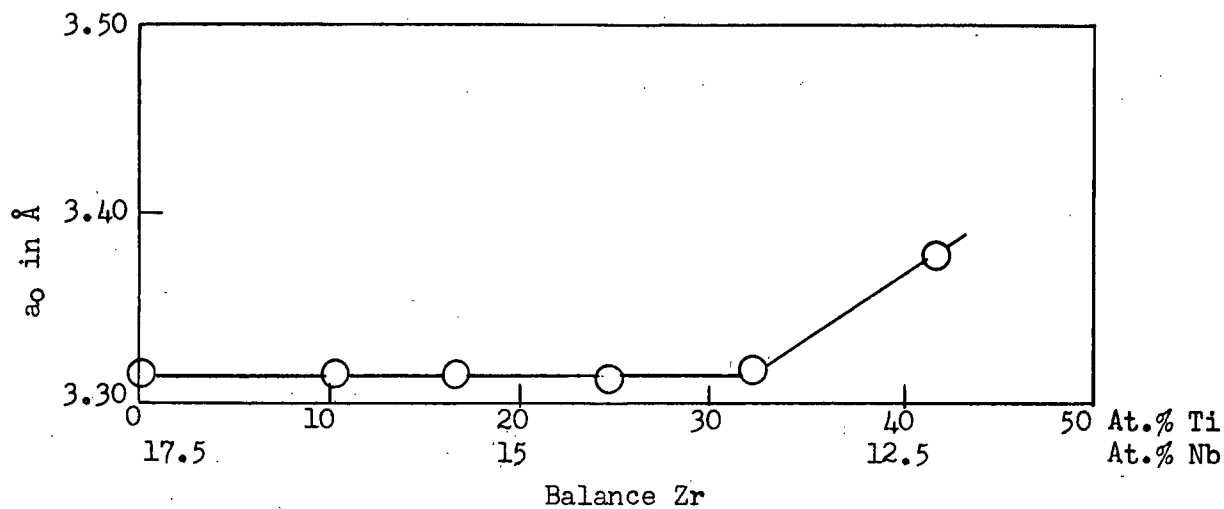


Figure 27. Variation of a_0 for β_{Nb} phase in monotectoid alloys of high niobium content at 450°C.

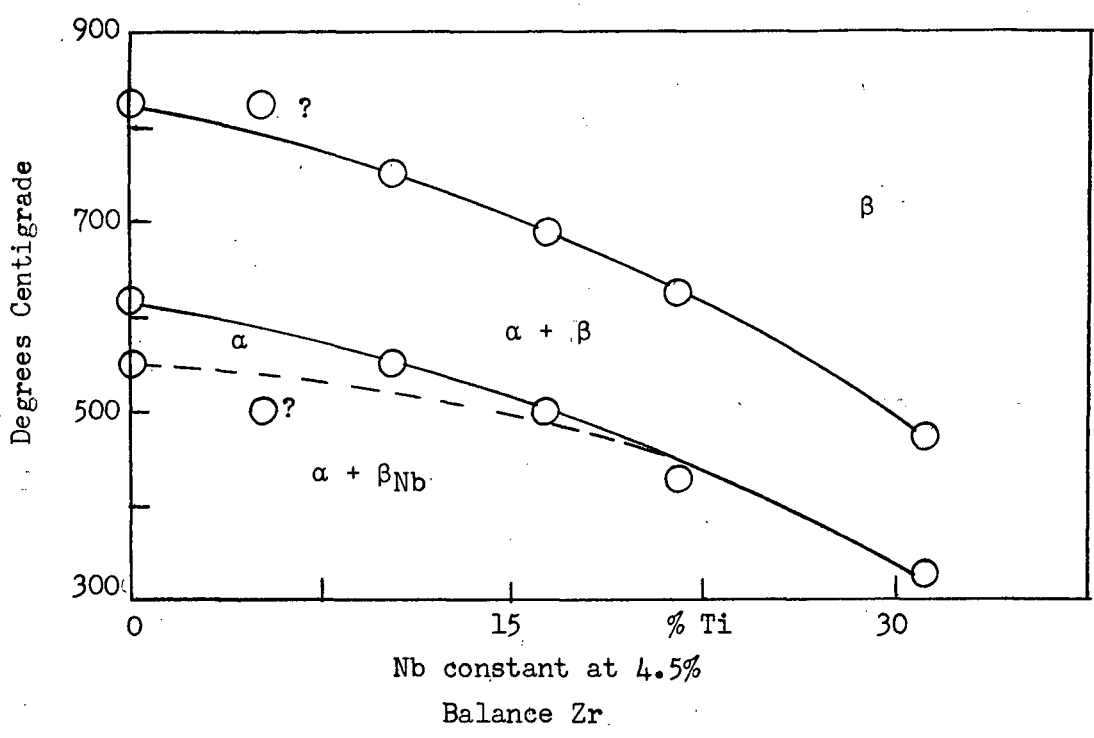


Figure 28. Ternary isopleth with niobium constant at 4.5 percent (temperatures corrected).

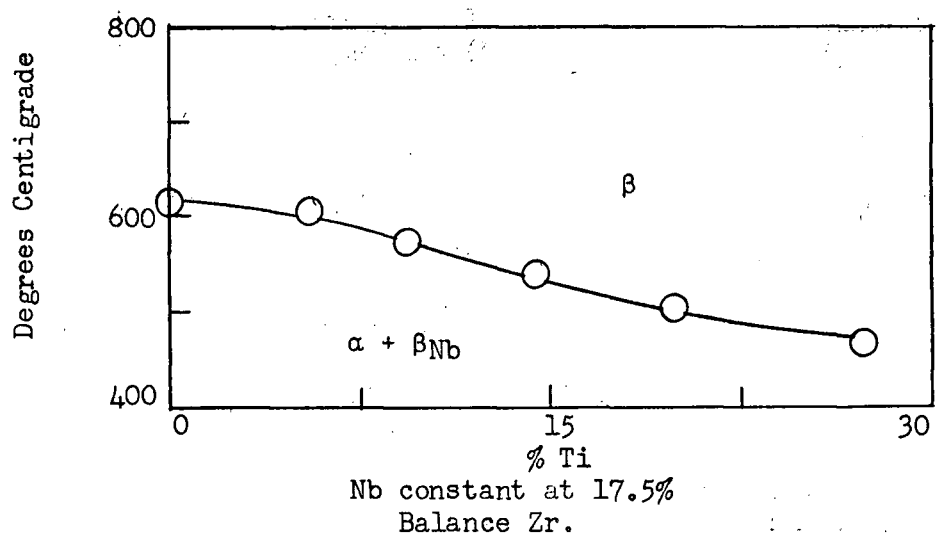


Figure 29. Ternary isopleth with niobium constant at 17.5 percent (temperatures corrected)

Appendix D contains the information obtained for one alloy. Sample scans of the type of reaction occurring in alloys of low niobium content are shown in Figure 30.

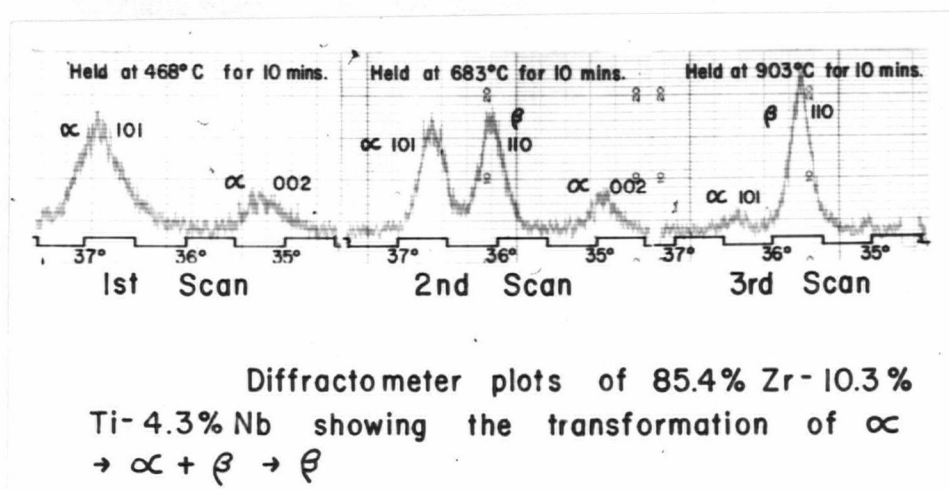


Figure 30 Sample scans showing the transformation of α to β .

The high niobium isopleth in Figure 29 was determined in much the same manner except that much longer times at temperature were required to make the reactions go to any extent. Figure 31 shows sample scans and all indicate that hysteresis was not too serious.

Both isopleths were constructed with corrected temperatures, that is, the error suggested by the silica powder temperature standardization run had been compensated for by subtracting 12°C from each experimentally determined temperature.

Figure 32 shows the growth of the unidentified phase mentioned earlier. The scans shown are those resulting from a direct experiment to determine the structure of the extra phase. When the phase was developed as much as possible, the specimen was rapidly cooled to room temperature and then an x-ray powder diffraction picture was taken. The phase was then tentatively identified as

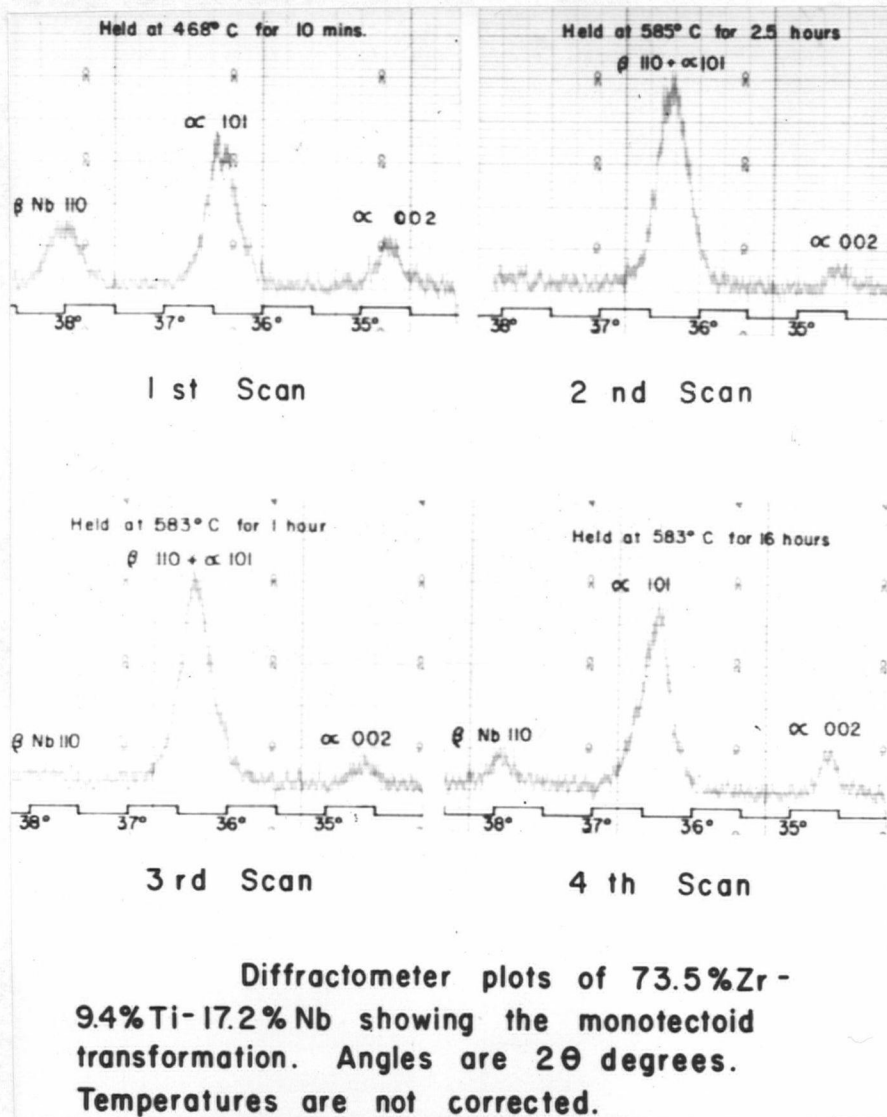


Figure 31. Sample scans showing the monotectoid transformation.

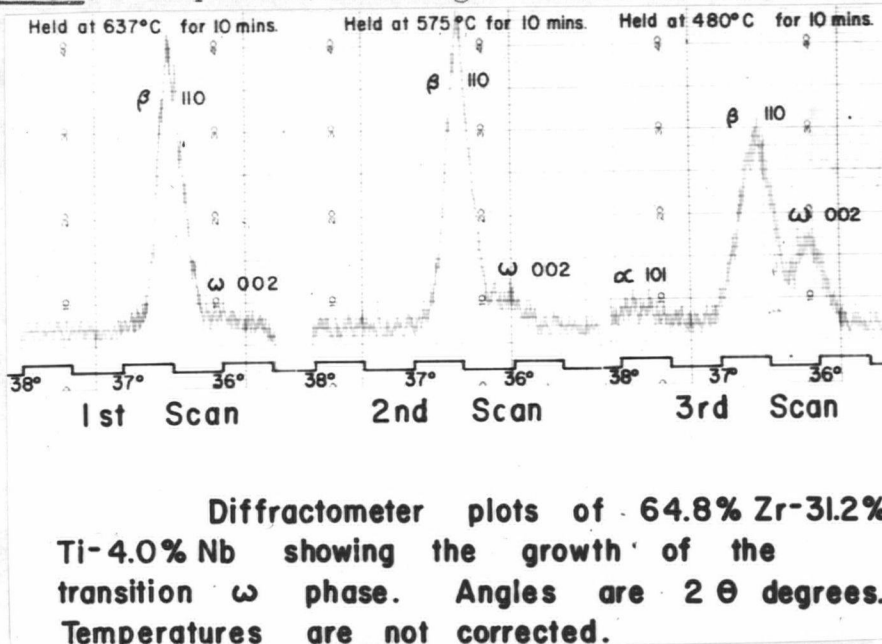


Figure 32. Sample scans showing the growth of the transition ω - phase.

being tetragonal with $a_0 = 3.85 \text{ \AA}$, $c_0 = 4.83 \text{ \AA}$, and $c/a = 1.25$

D. Ternary Isothermals.

Utilizing the ternary isopleths determined experimentally and the zirconium-niobium binary with the zirconium-titanium binary, a series of ternary isothermal sections for the zirconium-rich corner of the system can be approximated. The deficiencies of isothermal sections will be discussed in Section IV.

Figures 33(a) to (h) are the isothermal sections and portray the ternary diagram from 800°C to 450°C inclusive in 50°C steps.

IV DISCUSSION OF RESULTS AND CONCLUSIONS

No previous work could be found that would be useful as a guide in the interpretation of the results presented. However, a textbook by Rhines¹⁴ was very useful in sketching the isothermal sections in that it portrayed the shapes possible and pointed out impossible thermodynamic equilibria. Rhines also stated that very little was known about the mechanism and reaction rates of ternary eutectoid reactions. However, the analogy between binary eutectic-binary eutectoid and ternary eutectic-ternary eutectoid reactions appears to be good in all respects.

The principal source of unreliability in the results presented is the unknown level of contamination in the alloys. No gas analyses were obtained on the as-cast ingots and the heat-treated powders. One reference¹⁵ to gas contamination in the drip-melting of zirconium stated that within the accuracy of analytical methods, neither oxygen (200 ppm) nor nitrogen (5 ppm) was picked up when the metal was melted in a vacuum of 10^{-6} mm of mercury. As the high-temperature x-ray unit was operated at an equally good vacuum, it is felt that

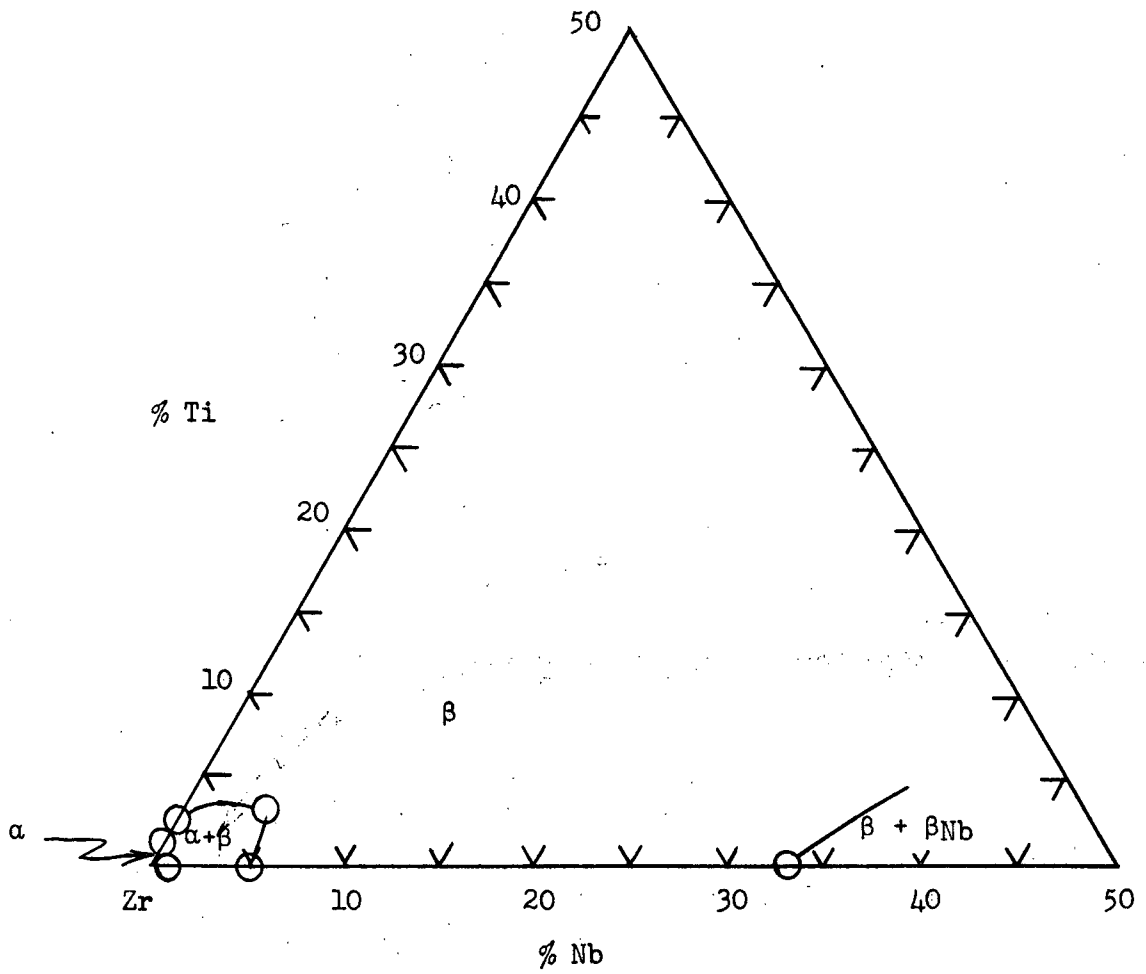


Figure 33(a) Isothermal section at 800°C.

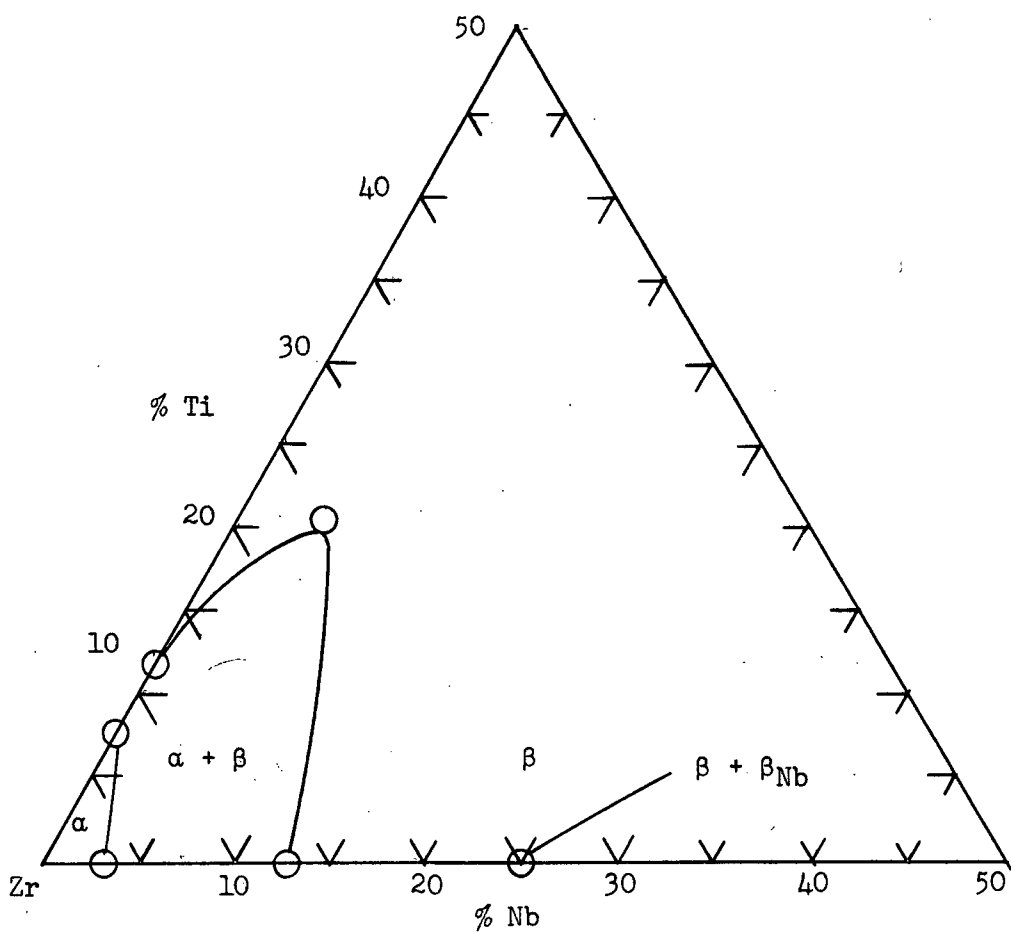


Figure 33(c) Isothermal section at 700°C.

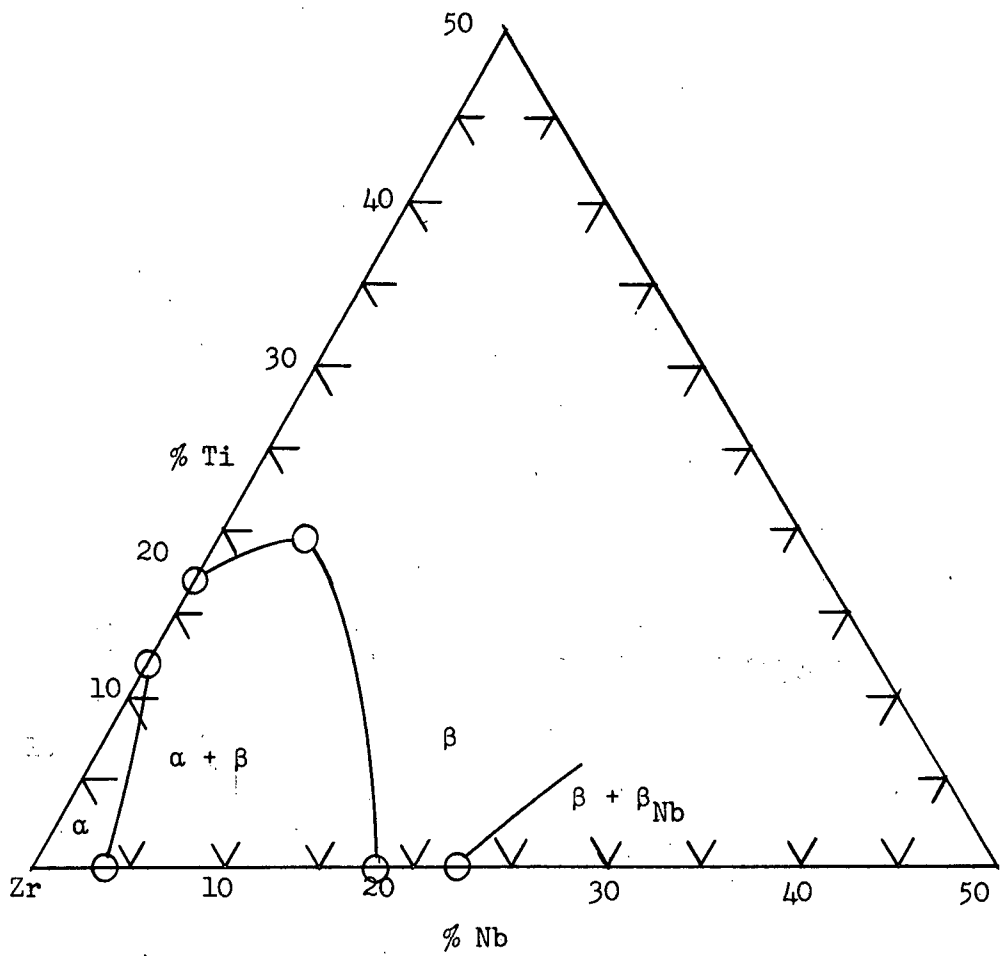


Figure 33(d) Isothermal section at 650°C.

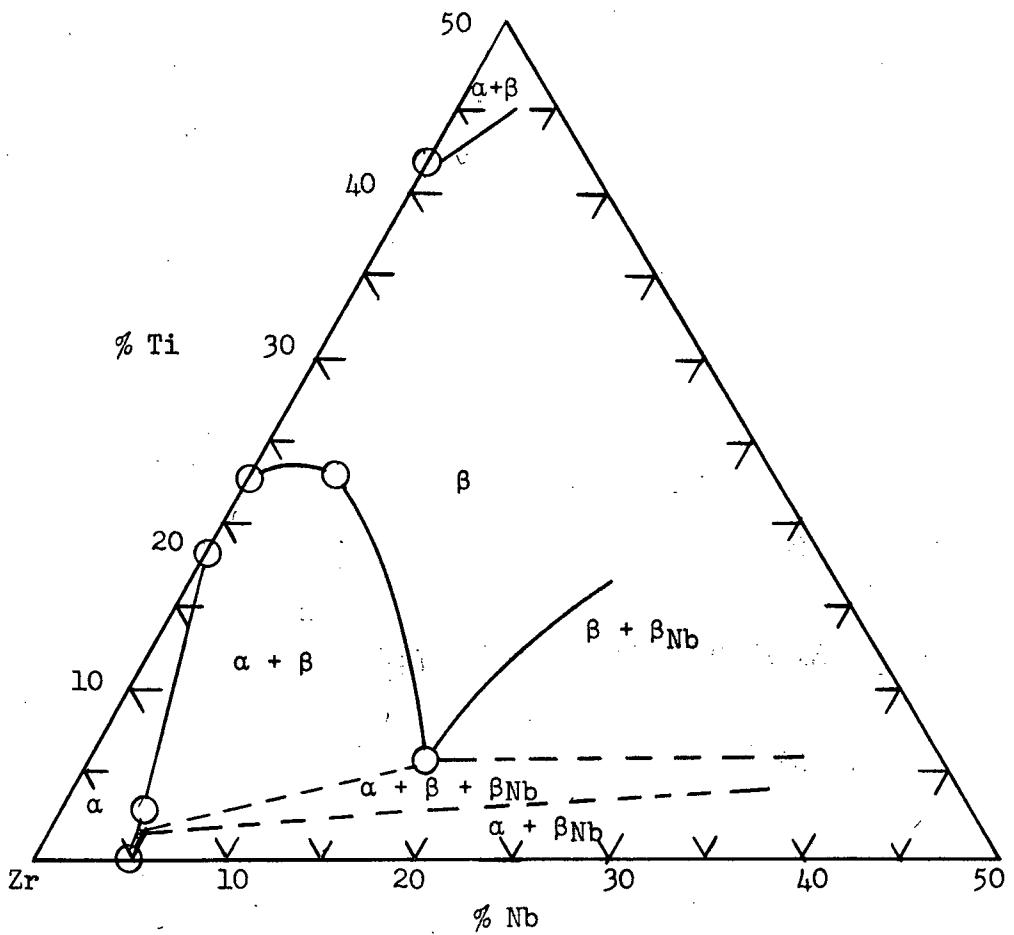


Figure 33(e) Isothermal section at 600°C.

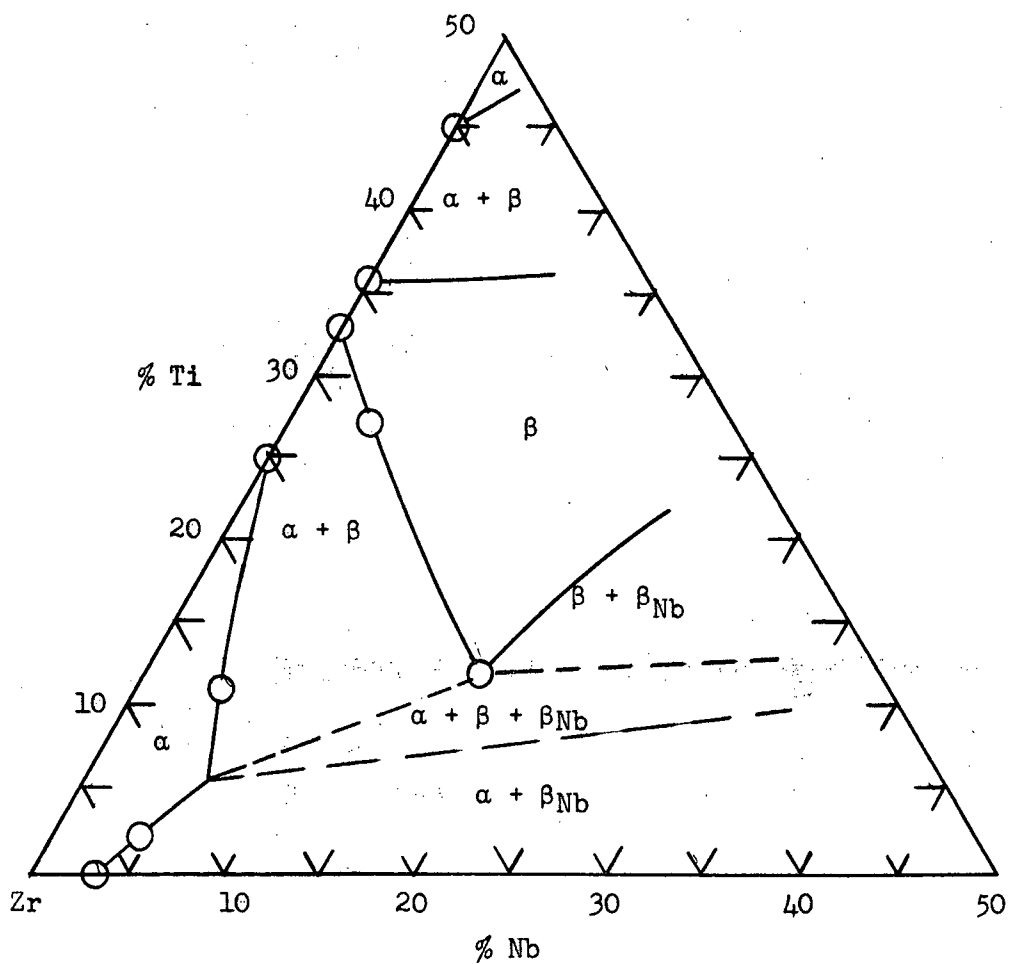


Figure 33(f) Isothermal section at 550°C.

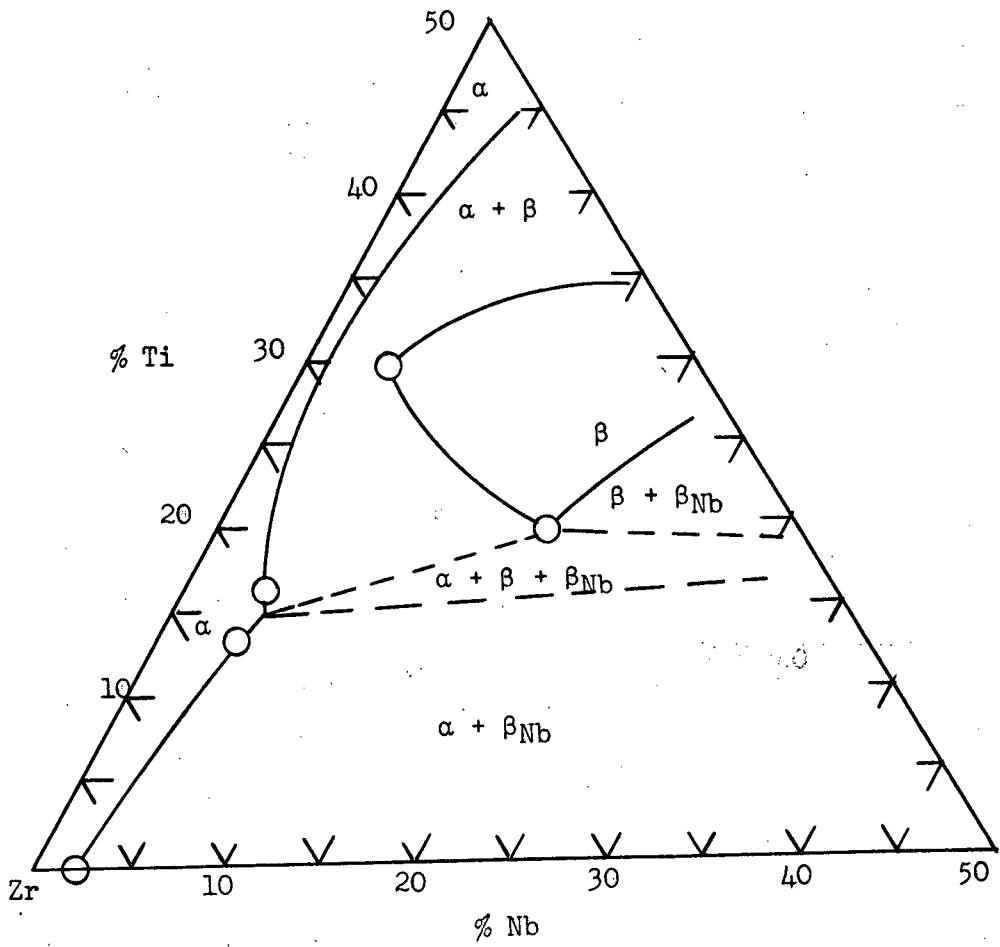


Figure 33(g) Isothermal section at 500°C.

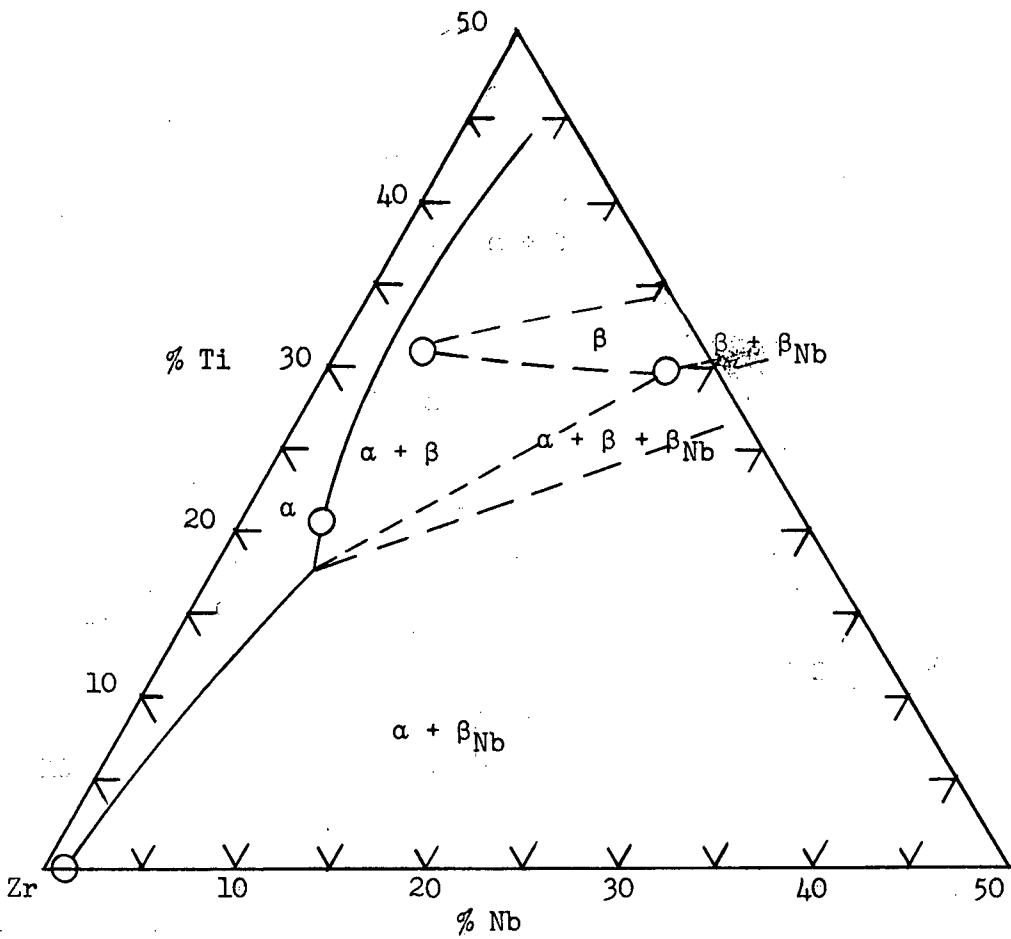


Figure 33(h) Isothermal section at 450°C.

gas contamination in the unit was not serious. Nevertheless, the relative gettering ability of powdered zirconium and molten zirconium is unknown and in addition, the powder was exposed to the vacuum at medium temperatures for some time (up to 24 hours) whereas the molten zirconium was in the active state for a matter of only one or two seconds. Gas analyses alone can settle the problem.

It should be noted that two points on the low niobium ternary isopleth are questioned. It is felt that these points were unreliable due to gas contamination. They were included to show the effect of contamination on the transformation temperatures.

The usefulness of the lattice parameters measured appears to be low and this is especially true of those obtained for the close-packed hexagonal phases. Firstly, in no x-ray pattern were the high-angle α -doublets resolved, as is considered necessary for accurate measurements. Secondly, Vegard's law does not appear to be obeyed, especially in the high niobium alloys. Thirdly, higher accuracies than were attained are required as differences in the fourth significant figure of the c/a ratio are important.

The β_{Nb} lattice parameters are considered to be good, for plots of the Taylor-Sinclair function versus lattice parameter show little random and systematic error. The β_{Nb} lattice parameter plots correlate very nicely with the determined isopleths as the parameters exhibit a change in linearity when they cross a phase boundary exhibited in the isopleths.

None of the plots of lattice parameters were of use in determining the isothermal section at 450°C as many more alloys would be required to construct accurate tie lines of isoparameters.

Further, the compositions of the precipitated phases in the monotectoid reaction were unknown and so their positions could not be located.

Finally, Brillouin zone effects,¹⁶ largely qualitative for alpha zirconium, may alter the c/a ratio as the amount of zone overlap changes. This would be sufficient to upset Vegard's law.

The metallographic results are too sparse to warrant much discussion. Chiefly, the data obtained correlate fairly well with the measured isopleths and thus suggest that the high-temperature powder technique is quantitatively useful for reactive metals.

The high-temperature x-ray unit failed in one respect in that no clear indication was obtained that a three-phase field ($\alpha + \beta + \beta_{Nb}$) existed under the monotectoid reaction plane. Such a field was not shown on the high niobium isopleth, but has been dotted in on the isothermal sections as an estimate to keep experimentally undetermined areas quite general.

The ternary isopleths as presented are felt to be quite accurate, although temperature limits of $\pm 10^\circ\text{C}$ must be placed on the points because of unavoidable hysteresis effects.

It should be emphasized that the isopleths do not represent equilibrium conditions in the sense that a binary diagram does. Tie lines in two phase areas joining points in equilibrium will lie in the plane of any given isopleth only by coincidence and then rarely. This is one of the conditions that a true quasi-binary must fulfill, and such is certainly not the case for the isopleths presented in this work.

One interesting phenomenon observed during operation of the high-temperature unit was the development of a metastable transition phase in two

high-titanium, low niobium alloys. The phase was eventually identified as being tetragonal and was called an ω -phase after the titanium notation already in force.

Such a transition phase has been observed in several titanium systems, principally the titanium-vanadium system¹⁷ where reversion and retrogression phenomena were also noted. Domagala et al¹⁸ make the first reference to any such transition phase occurring in zirconium-rich alloys. Perhaps such a transition phase would account for the unexplained extra lines observed by Rogers and Atkins⁷ and Hansen et al¹⁰ in their constitutional diagram work.

In this research, the so-called ω -phase was found to be reversible and its formation could be suppressed if a sufficiently low cooling rate were used. As the data being collected were to be based on equilibrium structures, any further ω formation was suppressed when encountered. However, some belief that it arises because of contamination exists and its true nature should therefore be more fully explored.

The isothermal sections constructed from the isopleths and the zirconium binaries are only of a qualitative nature. The true nature of the 450°C isothermal section is somewhat obscure and many more alloys would be required to outline the region of intermediate titanium content more accurately.

In conclusion, two isopleths have been determined for the zirconium-rich corner of the zirconium-titanium-niobium constitutional diagram. Lattice parameters for both phases of several monotectoid alloys at 450°C have also been measured but they were of limited usefulness due to a general lack of data in other regions of the ternary diagram. A high-temperature x-ray unit was designed which handled reactive zirconium alloy powders quite well up to temperatures of 1100°C. However, much more experimental work would be

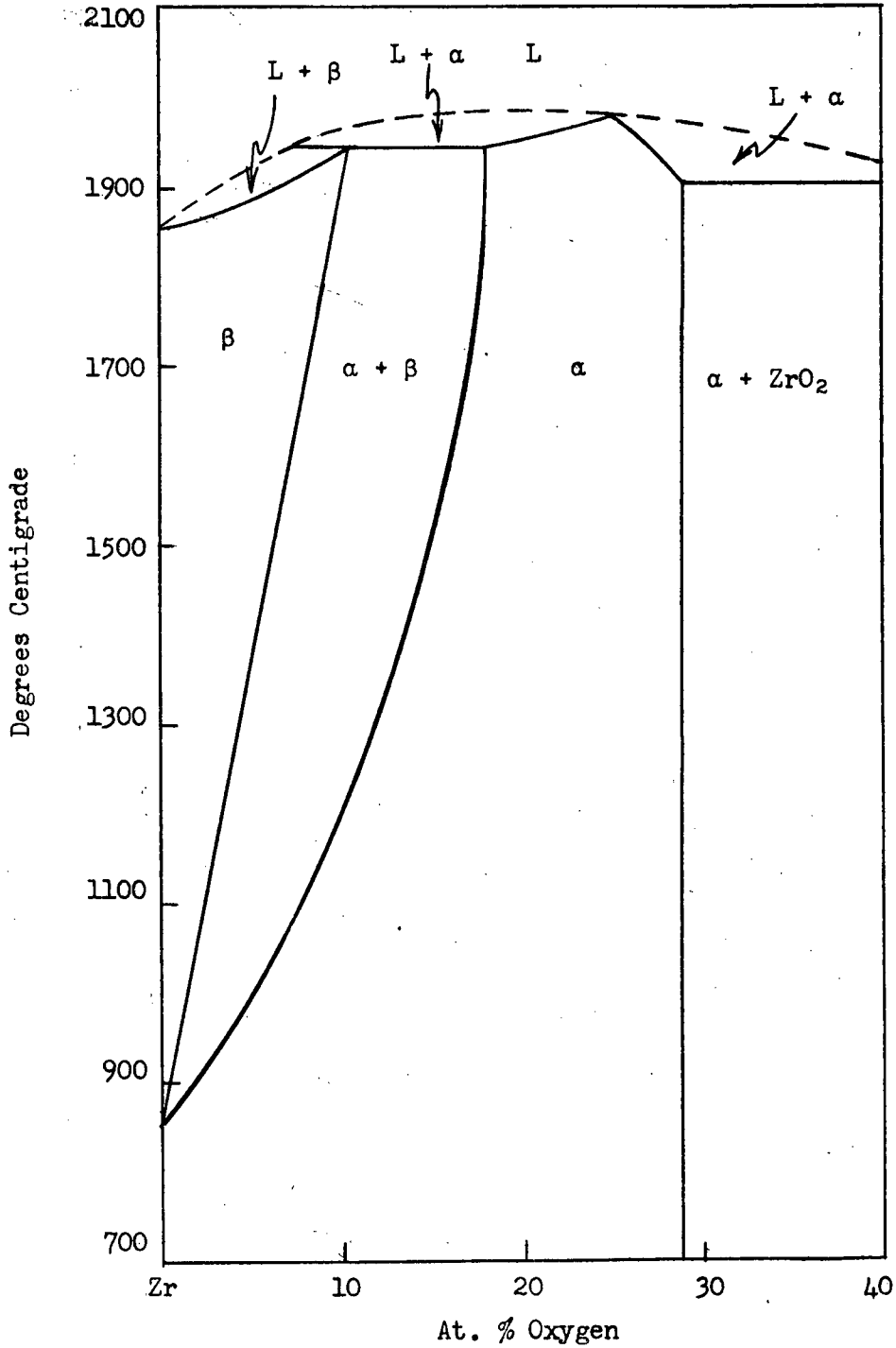
required before the ternary diagram could be accurately outlined and time-consuming techniques would be required.

V. RECOMMENDATIONS FOR FURTHER WORK

Further work on this ternary system must first check the results presented. It is felt that dilatometric studies would be very valuable though difficult to carry out. The resistometric technique described by Rogers and Atkins⁷ and modified by Finlayson⁹ would also give much information. Many more alloys would be required for a complete study of the zirconium corner and a knowledge of the contamination level would be essential for accurate work.

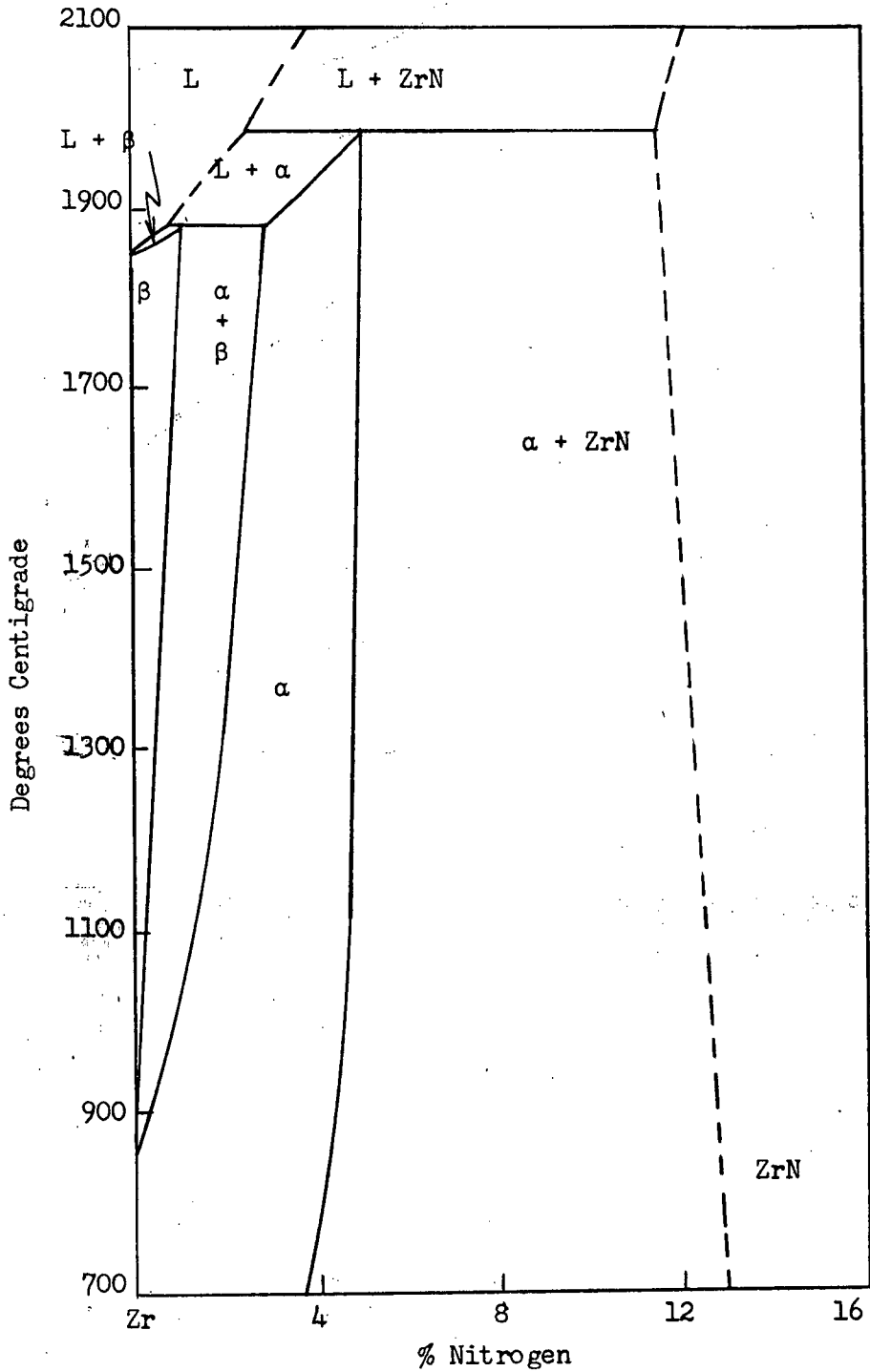
APPENDIX A

Related Binaries of Impurity Elements

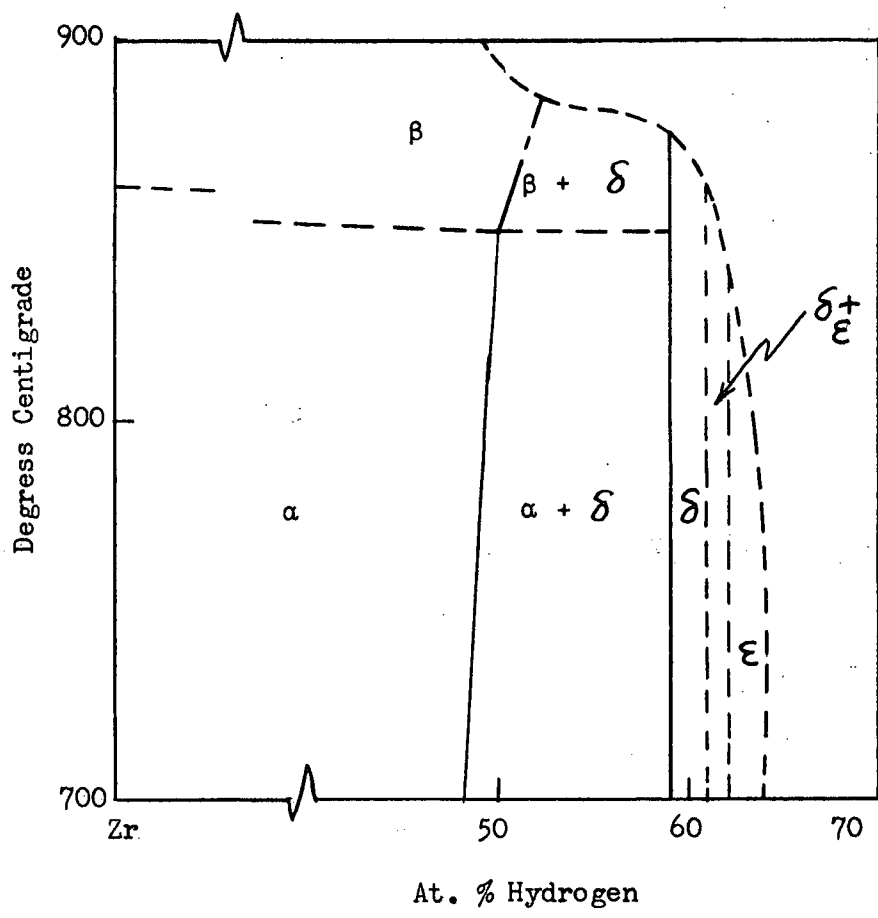


Zirconium-oxygen system
(after Hansen et al¹⁹)

APPENDIX A (continued)

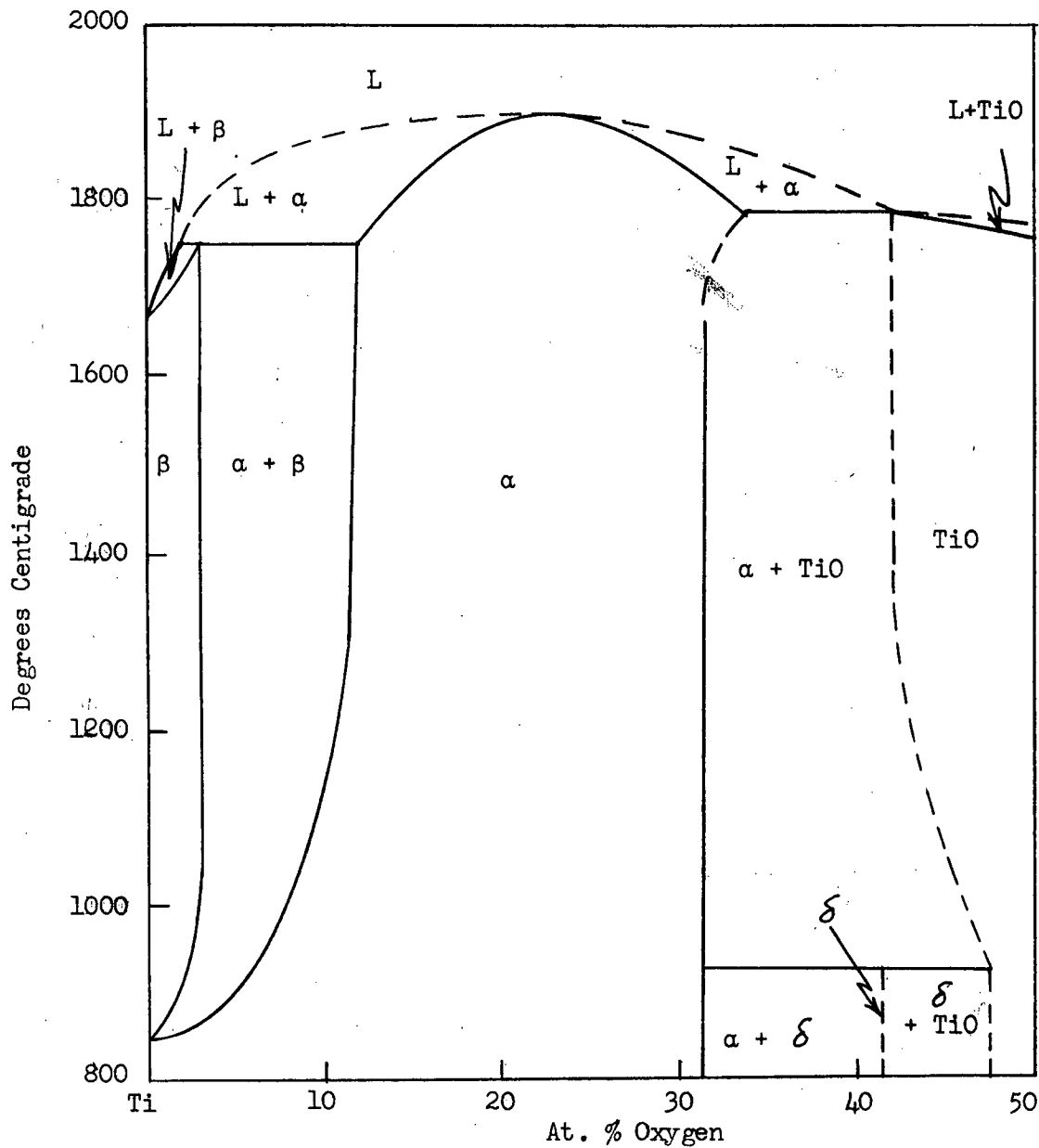


Zirconium-nitrogen system
(after Domagala and McPherson²⁰).



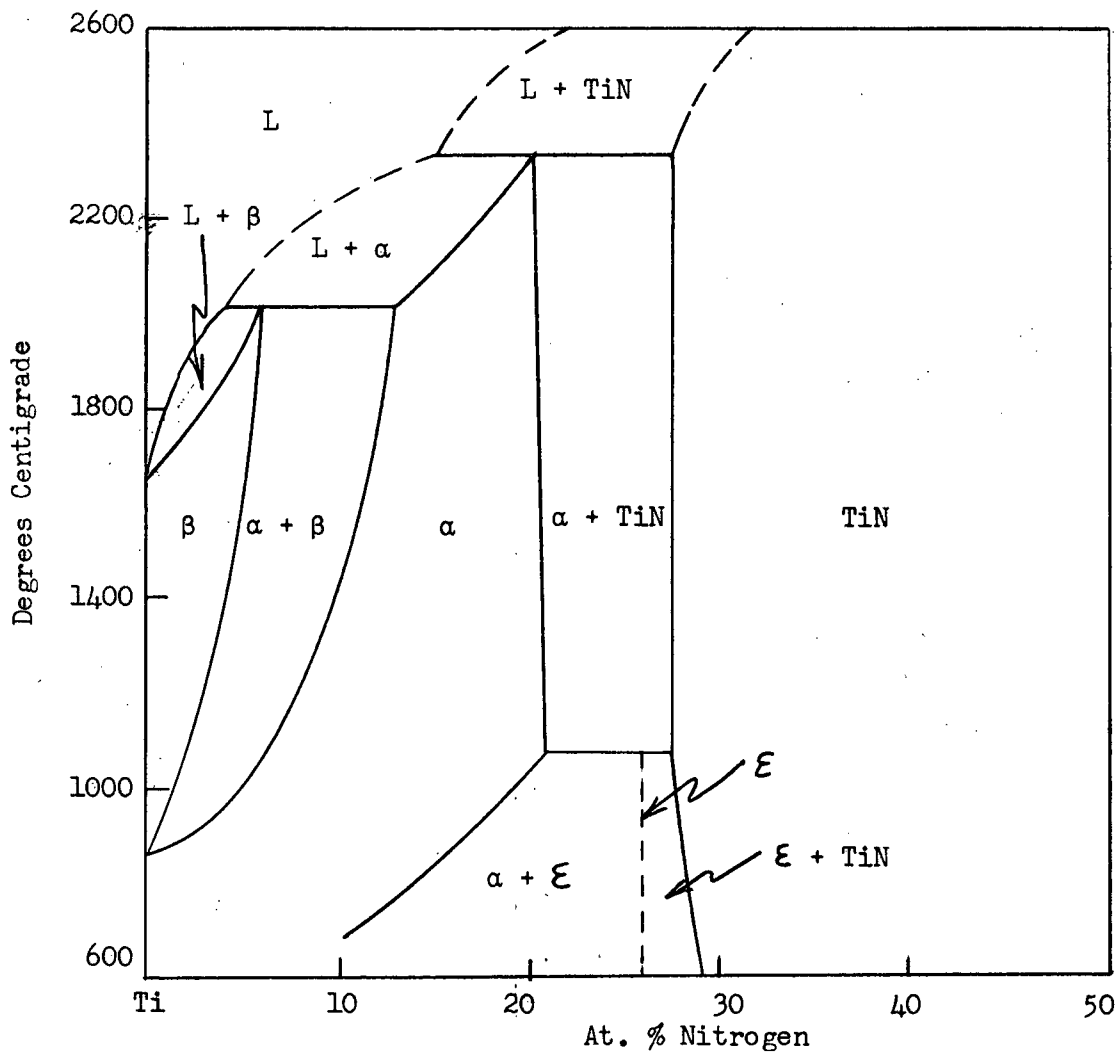
Zirconium-hydrogen system
(after Edwards et al²¹).

APPENDIX A (continued)



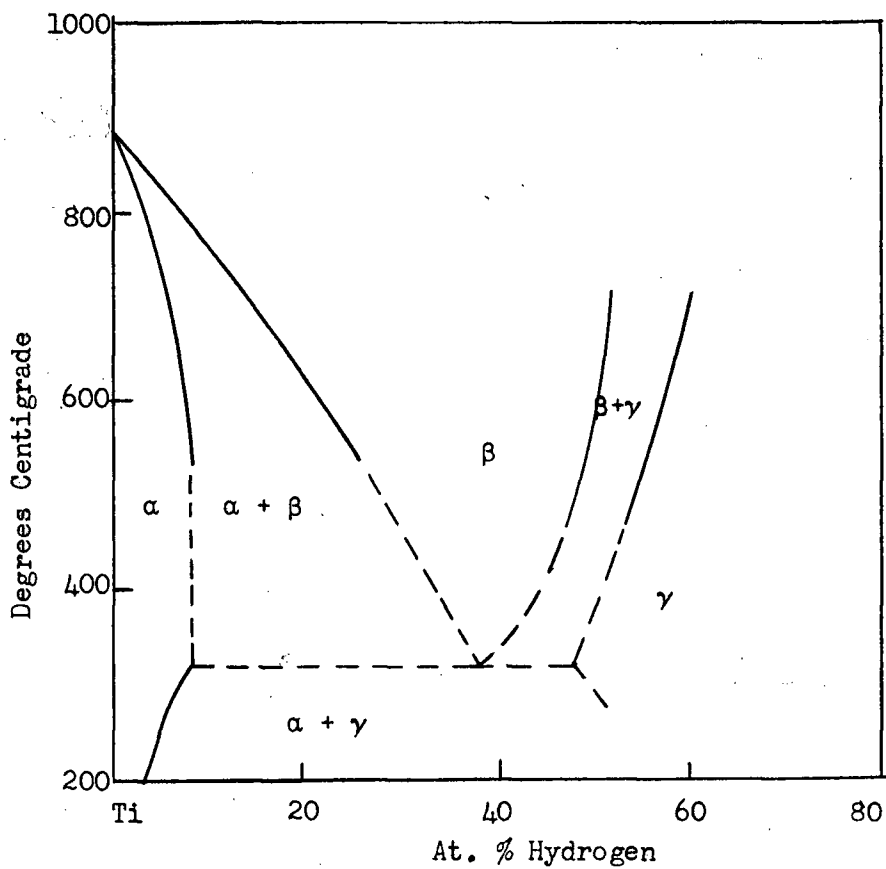
Titanium Oxygen System
(after Bumps et al²²).

APPENDIX A (continued)



Titanium-nitrogen system
(after Palty et al²³)

APPENDIX A (continued)



Titanium-hydrogen system
(a composite of several researches)

APPENDIX B

Lattice Parameter Calculation by the Method of Cohen

Cohen's method of determining lattice parameters is of most use when applied to noncubic substances, since straight forward graphical extrapolation cannot be used when there is more than one lattice parameter involved. Cohen's method provides a direct means of determining these parameters. For a hexagonal substance,

$$\sin^2 \theta \text{ (true)} = \frac{\lambda^2}{4} \cdot \frac{4}{3} \cdot \frac{h^2 + hk + k^2}{a_0^2} + \frac{\lambda^2}{4} \cdot \frac{l^2}{c_0^2}$$

$$\text{and } \sin^2 \theta - \frac{\lambda^2}{3a_0^2} (h^2 + hk + k^2) - \frac{\lambda^2}{4c_0^2} (l^2) = D \sin^2 \theta$$

if the pattern is made in a Debye-Scherrer camera. By rearranging the equation and introducing new symbols, we obtain

$$\sin^2 \theta = C\alpha + B\gamma + A\delta$$

$$\text{where } C = \frac{\lambda^2}{3a_0^2}, \alpha = (h^2 + hk + k^2), B = \frac{\lambda^2}{4c_0^2},$$

$$\gamma = l^2, A = \frac{D}{10} \text{ and } \delta = 10 \sin^2 2\theta$$

The values of C, B and A, of which only C and B are needed, are then found from the three normal equations:

$$\sum \alpha \sin^2 \theta = C \sum \alpha^2 + B \sum \alpha \gamma + A \sum \alpha \delta$$

$$\sum \gamma \sin^2 \theta = C \sum \alpha \gamma + B \sum \gamma^2 + A \sum \gamma \delta$$

$$\sum \delta \sin^2 \theta = C \sum \alpha \delta + B \sum \delta \gamma + A \sum \delta^2$$

For this work, four high angle lines were chosen (ie. the 213, 302, 205 and 106 planes) to make up the three normal equations. The a's and c's were then solved for.

APPENDIX C

d-Spacings of the α -Containing Alloys and the ω -Phase

All equilibrated to 450°C.

Index	NBS	.5.3% Ti .4.7% Nb	10.3% Ti 4.3% Nb	16.4% Ti 4.6% Nb	21.5% Ti 4.5% Nb
100 α extra	2.798	.2.762	2.749 2.677	2.743	2.725 2.662
002 α	2.573	2.538	2.517	2.584	2.503
101 α	2.459	2.425	2.415	2.409	2.394
110 β_{Nb}		2.328	2.328		2.394
102 α 003 α	1.894	1.873	1.865	1.860 1.692	2.394
200 β_{Nb}			1.650		1.700
110 α 103 α 200 α	1.616 1.463 1.399	1.599 1.448 1.384	1.590 1.441 1.377	1.585 1.435 1.378	1.579 1.425 1.367
211 β_{Nb}					1.388
112 α 201 α 004 α 202 α 104 α 203 α 210 α	1.368 1.350 1.287 1.230 1.169 1.084 1.059	1.355 1.338 1.275 1.219 1.160 1.077 1.049	1.348 1.331 1.268 1.211 1.150 1.069 1.046	1.346 1.327 1.261 1.208 1.146 1.066 1.041	1.336 1.320 1.252 1.203 1.142 1.059 1.034
310 β_{Nb}					1.077
211 α 114 α extra 212 α 105 α 204 α 300 α 301 α 213 α 302 α 006 α 205 α 106 α 220 α	1.036 1.006 .978 .966 .947 .933 .900 .877 .858 .829 .820	1.029 1.000 .986 .971 .959 .934 .927 .894 .871 .851 .824 .814 .803	1.022 .994 .965 .953 .935 .921 .889 .866 .844 .818 .807 .799	1.018 .988 .973 .960 .947 .925 .916 .905 .885 .862 .845 .814 .804 .794	1.014 .983 .958 .943 .930 .910 .881 .859 .811

APPENDIX C (continued)

All equilibrated to 450°C.

Index	NBS	5.6% Ti 17.6% Nb	9.4% Ti 17.2% Nb	14.4% Ti 17.0% Nb	19.8% Ti 17.1% Nb	27.3% Ti 17.4% Nb
100 α extra	2.798	2.769	2.768	2.754	2.744	2.731
002 α	2.573	2.540	2.539	2.531	2.522	2.512
101 α	2.459	2.434	2.429	2.419	2.409	2.399
110 β Nb		2.330	2.329	2.325	2.339	2.373
102 α extra	1.894	1.878	1.870	1.869	1.858	1.855 1.741
200 β Nb		1.652	1.649	1.649	1.656	1.683
110 α extra	1.616	1.606	1.600	1.593	1.588	1.584 1.524
103 α extra	1.463	1.452	1.450	1.492 1.446	1.437	1.432
200 α	1.399	1.389	1.381	1.381	1.375	1.375
112 α	1.368	1.361	1.355	1.352	1.348	1.343
201 α extra	1.350	1.340	1.337	1.334 1.304	1.328 1.301	1.324 1.298
004 α extra	1.287	1.278	1.273	1.272	1.264	1.263 1.263
202 α	1.230	1.221	1.219	1.214	1.208	1.206
220 β Nb		1.172	1.172	1.169	1.173	1.191
104 α	1.169	1.162	1.159	1.154	1.147	
203 α	1.084	1.077	1.075	1.072	1.067	
210 α	1.059	1.051	1.047	1.045	1.049	1.042
310 β Nb		1.045	1.047	1.045	1.049	1.066
211 α extra	1.036	1.029	1.028	1.024	1.020 1.003	1.018
114 α extra	1.006	1.001	.999	.995	.991	.987 .975
212 α	.978	.973	.970	.968	.964	.975
105 α	.966	.960	.958	.954	.951	.946
204 α	.947	.941	.939	.938	.932	.928
300 α	.933	.928	.926	.924	.919	
321 β Nb		.885	.885	.883	.887	.902
213 α	.900	.896	.893	.890	.887	.886
302 α	.877	.873	.870	.867	.864	.861
006 α	.858	.854	.851	.845	.842	.842
400 β Nb					.829	
205 α	.829	.825	.823	.819	.816	.816
106 α	.820	.819	.811	.808	.805	.803
220 α		.804	.802	.799	.796	.795

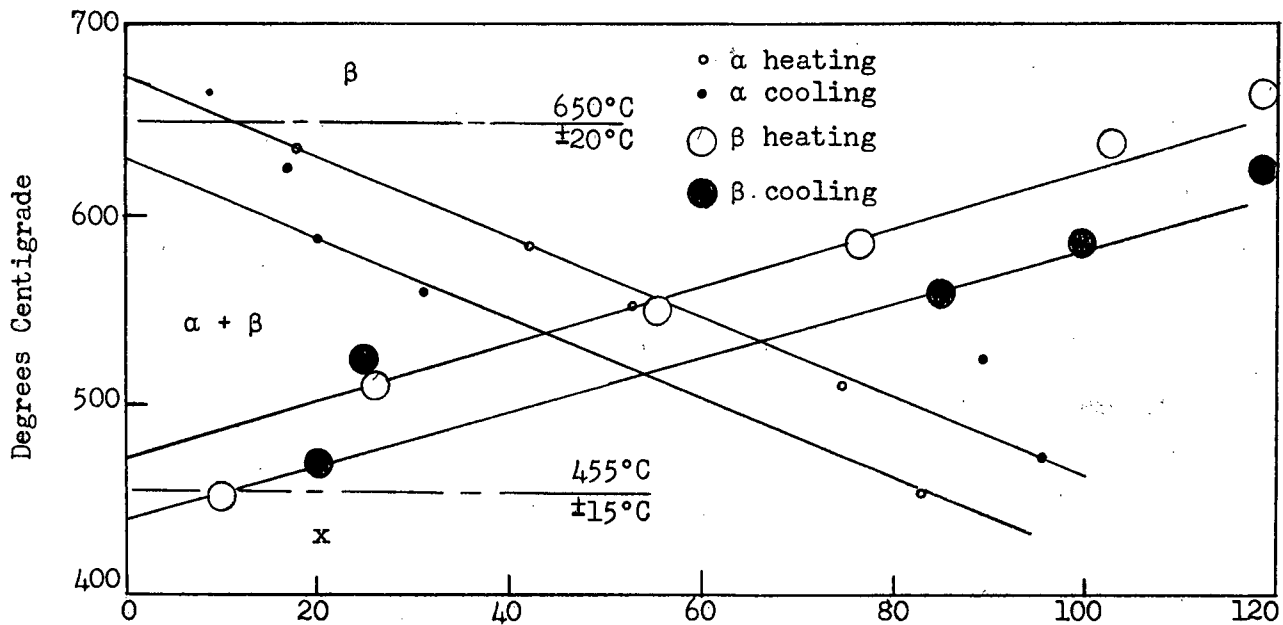
APPENDIX C (continued)

ω - Phase d - Spacings

Zr-Mo After Domalaga et al ¹⁸	Ti-V After Brotzen et al ¹⁷	31.2% Ti .4.0% Nb
3.154	2.74	3.041
2.309	2.28	2.453
2.204	1.626	1.909
1.967	1.398	1.734
1.908	1.317	1.519
1.636	1.202	1.410
1.571	1.151	1.288
1.335	.967	1.218
1.166	.915	1.094
1.068	.894	1.031
1.030	.871	.995
0.982	.850	.951
0.877	.799	.921
0.813		.857
		.812

APPENDIX D

Temperature Determination of Phase
Boundaries in One Low Niobium Alloy.
(74.0% Zr - 21.5% Ti - 4.5% Nb)



Peak Areas in Absolute Units as Measured with a K. and E. Polar Planimeter.

BIBLIOGRAPHY

1. B.D. Cullity, 'Elements of X-Ray Diffraction', Appendix 13, Addison-Wesley Publishing Company, Inc. (1956).
2. P.C.L. Pfeil, A Discussion of the Factors Affecting the Constitution of Zirconium Alloys, Report AERE-M/R-960, June 27, 1952.
3. P.C.L. Pfeil, A Critical Review of the Alloying Behaviour of Zirconium, Report AERE-M/TM-11, June 9, 1952.
4. J.D. Fast, The Transition Point Diagram of the Zirconium-Titanium System, Rec. Trav. Chim., 58:973, (1939).
5. E.T. Hayes, A.H. Roberson and O.G. Paasche, Zirconium-Titanium System: Constitutional Diagram and Properties, Bur. Mines Dept. Invest. 4826, November, 1951.
6. P. Duwez, Allotropic Transformation in Titanium-Zirconium Alloys, J. Inst. Metals, 80:525, (1952).
7. B.A. Rogers and D.F. Atkins, Zirconium-Columbium Diagram, Trans. A.I.M.E., 203:1034, (1955).
8. Yu F. Bychkov, A.N. Rozanov and D.M. Skorov, Atomnaya Energia, 2:146, (1955).
9. M.J. Finlayson, 'Isothermal Transformations in Eutectoid Zirconium-Niobium Alloys', M.A.Sc. thesis, University of British Columbia, (1957).
10. M. Hansen, E.L. Kamen, H.D. Kessler and D.J. McPherson, Systems Titanium-Molybdenum and Titanium-Columbium, Trans. A.I.M.E., 191:881, (1951).
11. M.K. McQuillan and A.D. McQuillan, 'Titanium', Chapt.10, 335, Butterworths Scientific Publications, (1956).
12. D.H. Polonis, R.G. Butters and J.G. Parr, Research, 7:No. 2, (1954).
13. R.G. Butters and J. Gordon Parr, Canadian Journal of Technology, 33:117, (1955).
14. F.N. Rhines, 'Phase Diagrams in Metallurgy', McGraw-Hill Book Company, Inc., (1956).
15. B. Lustman and F. Kerze, Jr., Editors, 'The Metallurgy of Zirconium', Chapt.6, 247, McGraw-Hill Book Company, Inc., (1955).
16. B. Lustman and F. Kerze, Jr., Editors, 'The Metallurgy of Zirconium', Chapt.9, 433, McGraw-Hill Book Company, Inc., (1955).
17. F.R. Brotzen, E.L. Harmon, Jr. and A.R. Troiano, Decomposition of Beta Titanium, Trans. A.I.M.E., 203:413, (1955).
18. R.F. Domagala, D.W. Levinson and D.J. McPherson, Transformation Kinetics and Mechanical Properties of Zr-Mo Alloys, 209:1191, (1957).

Bibliography (continued)

19. M. Hansen, D.J. McPherson and R.F. Domagala, Phase Diagrams of Zirconium-base Binary Alloys, Report COO-123, (1953).
20. R.F. Domagala and D.J. McPherson, Armour Research Foundation, Project B017, Report 14, (1954).
21. R.K. Edwards, P. Levesque and D. Cubicciotti, Ill. Inst. of Tech., ONR Project 358-070, Report 13, (1953).
22. E.S. Bumps, H.D. Kessler and M. Hansen, Trans. A.S.M., 45:1008, (1953).
23. A.E. Palty, H. Margolin and J.P. Nielsen, Trans. A.S.M., 46:312 (1954).